# NUMERICAL MODELLING OF SUBMARINE LANDSLIDE IMPACT ON OFFSHORE FREE-SPANNING PIPELINES

by

**© DIPONKAR SAHA**

A thesis submitted to the

School of Graduate Studies

in partial fulfilment of the requirements for the degree of

**Master of Engineering (Civil Engineering)**

**Faculty of Engin**eering **a**nd Applied S**c**ience

Memorial University of Newfoundland

May, 2019

St. John's Newfoundland Canada

# ABSTRACT

Offshore pipelines are one of the most efficient and reliable modes of transportation of oil and gas. In shallow water conditions, the common practice is to bury the pipeline through trenching and backfilling. However, in deep water environments, pipeline burial through trenching is not very practical or cost-effective; therefore, the pipelines are often laid on the seafloor. Depending upon topography and seafloor environments, sections of as-laid (or surface-laid) pipelines might transform into the free-spanning pipeline. The suspended section of the pipeline might experience the impact of submarine landslides those frequently occur in continental slopes. The impact of debris flow, which originates from submarine landslides and travels in the downslope direction at high speed, might cause severe damage and even break out of these pipelines.

Quantifying the impact forces on free-spanning pipeline sections is one of the key requirements in the design. In the present study, debris flow impact is numerically modelled using two software packages: (i) Abaqus finite element (FE) and (ii) ANSYS CFX based on a Computation Fluid Dynamics (CFD) approach. Implementing appropriate models for soil and water together with new approaches for modeling pipe–soil–water interface behaviour, the process of impact, including soft clay flow around the pipe, is successfully simulated using the above-mentioned approaches. Overall, the modelling of this large deformation process is computationally expensive. However, the CFD approach in ANSYS CFX is more computationally efficient than the Coupled Eulerian-Lagrangian (CEL) approach in Abaqus FE software. The role of free-water suction in the channel behind the pipe, the effects of seabed shear strength and gap between pipeline and seabed on drag force are investigated. The drag force depends on not only the shear strength of the debris but also soil flow mechanisms around the pipe, which is influenced by the gap and seabed shear strength.

# ACKNOWLEDGEMENTS

At first, I want to express my immense gratitude to the Almighty for my good health and well-being throughout my research period.

This research work was supervised by Dr. Bipul Hawlader, Professor, Memorial University of Newfoundland, Canada. I want to express my utmost gratitude to him for his sincere and selfless support, prompt and useful suggestions and guidance during my research. I would also like to extend my sincere gratitude to Dr. Ashutosh Dhar, Assistant Professor, Memorial University of Newfoundland, Canada, who was my co-supervisor, for his continuous support, guidance, remarks, and engagement throughout my research, and writing this thesis. Without their immense support and continuous guidance, this thesis would not come into light.

I would like to thank the School of Graduate Studies of Memorial University of Newfoundland, Natural Sciences and Engineering Research Council (NSERC), Mitacs, Petroleum Research Newfoundland and Labrador (PRNL) and Equinor (formerly Statoil) Canada for providing me financial support for last two years.

I would also like to convey my sincere gratitude to Dr. Sujan Dutta, Dr. Kshama Roy and Binoy Debnath for their precious advice, guidance and assistance that accelerated the progress of my research. Special thanks to Munmun Sarkar and the little kid, Rishva Eha Dey for continuous moral support and entertainment through this long journey. My sincerest thanks go to my friends and well-wishers who directly or indirectly helped me in my research work.

Lastly, I am greatly indebted to my parents and my beloved wife for their unconditional love, care, affection and emotional support that made me go through all the hardship of these two years of graduate life. Without their support, I would not be able to complete my research.

# Table of Contents

# List of Figures

# List of Tables

# List of Symbols

| | |
|---|---|
| $A$ | projected frontal area |
| $C_D$ | drag coefficient |
| $C_L$ | lift coefficient |
| $D$ | pipe diameter |
| $D_e$ | effective pipe diameter |
| $D_o$ | outside pipe diameter |
| $F_x$ | horizontal component of drag force |
| $f$ | geometric tension factor |
| $f_1$ | factor for strain rate effect on undrained shear strength |
| $f_2$ | factor for strain-softening effect on undrained shear strength |
| $g$ | gap between the pipe and seabed |
| $\hat{g}$ | normalized gap between the pipe and seabed |
| $F_D$ | drag force on pipe—if not specified, normal to the pipe axis |
| $F_{D,90}$ | drag force component normal to the pipe axis |
| $F_{D,0}$ | drag force component parallel to the pipe axis |
| $k$ | drag force parameter in geotechnical approach |
| $L$ | length of pipeline segment affected by landslide |

| | |
|---|---|
| $\Delta L$ | elongation of pipeline |
| $N_c$ | bearing capacity factor |
| $N_h$ | normalized horizontal drag force |
| $N_{h(max)}$ | maximum normalized horizontal drag force |
| $p$ | pressure |
| $Re_{Newtonian}$ | Reynold's number for Newtonian fluids |
| $Re_{non\text{-}Newtonian}$ | Reynold's number for non-Newtonian fluids |
| $s_u$ | mobilized undrained shear strength |
| $s_{uN}$ | undrained shear strength used for normalization |
| $s_{u0,d}$ | initial undrained shear strength of debris |
| $s_{u0,b}$ | initial undrained shear strength of seabed |
| $S_t$ | remoulded sensitivity |
| $S_\varphi$ | source term |
| $t_i$ | average thickness of element around the pipe |
| $u$ | lateral penetration |
| $\hat{u}$ | normalized lateral penetration |
| $U_\infty$ | upstream velocity of debris flow |
| $v_0$ | initial velocity of debris flow |

$w$ depth of embedment of pipe

$\hat{w}$ normalized depth of embedment of pipe

$\alpha$ adhesion factor

$\xi$ magnitude of accumulated plastic shear strain

$\xi_{95}$ value of $\xi$ at 95% reduction of shear strength of soil due to remoulding

$\rho$ density of flow (debris)

$\mu$ absolute (dynamic) viscosity

$\mu_{app}$ apparent viscosity

$\mu_d$ dynamic viscosity

$\tau$ shear tress

$\dot{\gamma}$ Strain rate

$\dot{\gamma}_{ref}$ reference shear strain rate

$\gamma_p$ plastic shear strain

$\gamma'$ submerged unit weight of soil

$\theta$ initial angle between the pipeline axis and seabed contour

# Chapter 1

# Introduction

## 1.1 General

The rapidly growing demand for hydrocarbon production dictates rapid development of offshore technologies. To ensure an efficient and safe mode of transportation of hydrocarbons from the offshore to the onshore is a big challenge. Oil and gas pipelines play a major role in transporting the hydrocarbons in an effective way. In offshore environments at shallow water, it is a common practice to lay the pipelines in a trench and backfill it. These pipelines are then termed as "buried" pipelines. However, trenching in deep water environments is very expensive and to minimize the cost, pipelines are kept as-laid on the seafloor (often termed as "surface-laid" pipelines). These as-laid pipelines may penetrate partially into the soft seabed due to the self-weight and weight of the hydrocarbons. Then they are termed as "partially embedded" pipelines. Moreover, the surface-laid pipelines might pass through zones with uneven topology and some segments of the pipe might be hanging between two high points on the seabed which leads to free-spanning of pipelines. These pipelines are then termed as "suspended" pipelines. Free spanning of pipelines can be caused by the change of seabed topology due to scouring and wave actions, strudel scours, iceberg scar, artificial supports, rock beams or existence of pipeline crossings (DNV 2006). Figure 1.1 illustrates various scenarios that may lead to free-spanning of offshore pipelines. These pipelines might experience large ground movement impacts, such as due to submarine landslides. The failed soil mass, originating from a landslide, undergoes a lot of transformation through interaction with water and seabed while traversing in downslope direction. It may traverse hundreds of kilometers along the continental slope and transform into a debris flow. This debris can impact the seafloor structures, such as offshore telecommunication cables and oil and gas pipelines, on its way. In

order to prevent the breakout of these seafloor structures, they must be designed to withstand the thrust generated by the debris flow impacts on them. Estimating the loads on the seafloor structures due to the debris flow impact is always a challenging task. Current study attempts to develop a numerical modelling technique to quantify the drag force on the pipelines in a more accurate and computationally efficient way. Only suspended pipelines are considered in this study, while surface-laid, partially embedded or buried pipelines are beyond the scope of this study.

## 1.2 Objectives

The aim of this study is to understand the soil flow mechanisms and the role of suction that develops in the "free-water" in the channel which forms behind the pipe during the submarine landslide impacts on suspended pipelines. As typical Finite Element (FE) tools in the Lagrangian framework cannot model the large deformation phenomena due to mesh distortion issues, the analyses conducted in the present study using the Coupled Eulerian-Lagrangian (CEL) technique available in Abaqus 6.14 FE software and a Computational Fluid Dynamics (CFD) approach in ANSYS CFX software. At first, the computational efficiency of the two software packages has been compared through modelling a large deformation problem considering ideal soil behaviour (i.e. without considering strain-softening and strain-rate effects on the undrained shear strength). Later, the more computationally efficient software package is further used to investigate the soil flow mechanisms and variation of force-displacement behaviour for different gaps between the pipe and seabed, and undrained shear strength of seabed and debris while considering the strain-softening and strain-rate effects on clay shear strength.

## 1.3 Outline of thesis

The outcome of this research is presented in this thesis in five chapters. The first chapter provides with a brief introduction and main objectives of the research along with the contribution of this research towards offshore mechanics.

**Chapter 2** summarizes the previous studies conducted to analyze lateral pipe-soil interaction that occurs during submarine landslide impact on offshore pipelines. The development of analytical solutions, results of physical tests and numerical analyses are discussed here. Moreover, the limitations of previous studies related to suspended pipe-soil interaction are summarized in this chapter.

**Chapter 3** discusses the finite element and finite volume modelling techniques for large deformation problems. Finite element and finite volume results are compared to the guidelines and values obtained from previous numerical and analytical analyses. The effects of pipe–soil interface conditions on drag force on the pipe are investigated. Based on computational efficiency and advantage of modelling suction, the finite volume method is suggested for better modelling the problems considered in the present study. A part of the work presented in chapter 3 has been published as: Saha, D., Hawlader, B., Dutta, S. and Dhar, A. (2018) "A comparison using two numerical approaches for modelling the impact of submarine landslides on suspended pipelines," GeoEdmonton 2018, September 23–26, 2018, Edmonton, Alberta, Canada.

**Chapter 4** investigates the effects of the undrained shear strength of the seabed and debris, and gap between the pipe and seabed on the drag force generated during the impact of debris on a suspended pipeline. ANSYS CFX has been used for the numerical simulations. In this chapter, to capture a more realistic soil behaviour, strain-softening and strain-rate effects on clay shear

strength are considered. A parametric study is conducted to illustrate the effects of seabed strength and gap beneath the suspended pipe on drag force estimation.

Finally, **Chapter 5** summarizes the conclusions of this research. The limitations of the present study and recommendations for future research are also discussed in this chapter.

## 1.4 Contribution to offshore pipeline engineering

- Development of numerical modelling techniques to simulate pipeline–soil–water interaction during submarine landslides
- Analysis of soil behaviour and effects of free-water suction during large deformation using finite element and finite volume techniques
- Investigating and identifying the effects of gap and seabed strength on drag force caused by submarine landslide impact on offshore suspended pipelines.

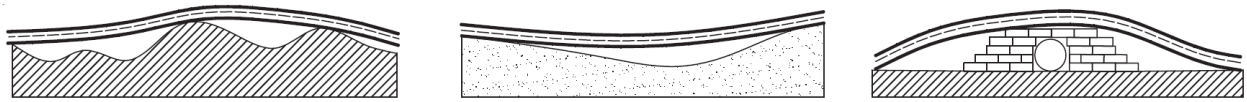

(a) (b) (c)

**Figure 1.1.** Various scenarios related to free-spanning: (a) seabed unevenness, (b) scouring at seabed and (c) pipeline crossing (after Drago et al. 2015).

# Chapter 2

# Literature Review

## 2.1 General

The offshore pipelines used to transport hydrocarbon in deep water (water depth > 400 m) are usually laid on the continental slopes without any trenching due to very high trenching cost and deep-water operational difficulties. These as-laid offshore pipelines often convert into suspended (free-spanning) pipelines due to seabed undulations, seabed scours, undulations caused by iceberg scars or existence of other seafloor structures (Fig. 2.1). As numerous small to large-scale landslides frequently occur in the offshore environment, these suspended pipelines may experience a large impact force caused by the downslope movement of a failed soil mass originating from submarine landslides. For example, the greatest landslide in Canadian history, the Grand Bank landslide in 1929, involved downslope movement of 100–150 $km^3$ of sediments (turbidity current) that travelled more than hundred kilometers and damaged the transatlantic telecommunication cables installed on the seafloor (Piper et al. 1999; Fine et al. 2005). This study aims at proper quantification of drag force caused by the debris flow impact on the suspended pipelines and finding out the factors affecting the drag force.

## 2.2 Phases of submarine landslides

The submarine landslide and associated mass movement is a complex phenomenon. When a failed soil mass, originating from the landslides, moves in the downslope direction, it undergoes significant remolding and fluidization processes resulting in the decrease of shear strength of the sliding soil mass. Depending on the remolded shear strength and distance travelled by the failed soil mass, various terminologies have been introduced (Mulder and Alexander 2001; Boylan et al.

2009; Pie et al. 2015). Figure 2.2 illustrates the phases of submarine landslides. Various terminologies introduced by different researchers are briefly discussed below (Zakeri and Hawlader 2013):

(a) *Glide block*: an intact block of soil mass during very early stage of landslide that has not been remolded and still carries the shear strength properties of the parent soil.

(b) *Out-runner block*: an intact block of cohesive sediment that has not been remolded and carries the shear strength properties of the parent soil but detached from the parent soil mass due to hydroplaning during the downward movement.

(c) *Debris flow*: a fully remolded and fluidized, high-density cohesive sediment that consists of a combination of solids and fluids with a minimum sediment concentration of 50% by volume. The material behavior of debris flow can be represented by rheological properties of non-Newtonian fluids.

(d) *Turbidity current*: a flow of sediments consisting of combination of sandy or clayey materials and fluids with sediment concentration less than 50% by volume. The behavior of turbidity current can be represented by rheological properties of a Newtonian fluid having a density higher or lower than the seawater.

The present study is focused on the impact of debris, which has initial undrained shear strength (without the effects of strain rate and strain-softening) ($s_{u0,d}$) of 1–10 kPa, on suspended pipelines. Other types of sediment flow are out of the scope of this study.

## 2.3 Lateral pipe–soil interaction

Considerable number of studies have been conducted in the past on lateral pipe–soil interaction for estimation of lateral force/resistance when a pipeline is subjected to lateral movement relative

to surrounding soil. The pipe–soil interaction during the debris flow impact is different from the process involves in typical buried pipeline—for example, the debris are generally very soft and moves significantly large distance and engulfs the pipe. The available approaches to quantify the drag force on a pipeline can be categorized into two groups: geotechnical approach and fluid mechanics approach. In the geotechnical approach, the drag force on the pipe is a function of the projected frontal area and the undrained shear strength of the impacting clay sediments (Audibert and Nyman 1977; Demars 1978; Bea and Aurora 1982; Swanson and Jones 1982; Summers and Nyman 1985; Georgiadis 1991; Zhu and Randolph 2009). A typical equation to quantify the drag force in geotechnical approach is:

$$F_D = k \times s_u \times A \tag{2.1}$$

where, $F_D$ is the drag force, $k$ is the model parameter (dependent on the shear strain rate), $s_u$ is the undrained shear strength of the impacting clay sediments, and $A$ is the projected area in the flow direction which eventually equals to the diameter of the pipe when unit length is considered. On the other hand, in the fluid mechanics approach, the debris is considered as a non-Newtonian fluid, and the drag force is a function of a drag coefficient, and density and velocity of the sliding sediments. Pazwash and Robertson (1975) adopted this approach for the first time and proposed the following formula to estimate the drag force:

$$F_D = \frac{1}{2} \times \rho \times C_D \times U_\infty^2 \times A \tag{2.2}$$

where, $\rho$ is the density of the flow, $C_D$ is the drag coefficient, $U_\infty$ is the upstream velocity of flow and $A$ is the projected frontal area as in the previous approach. When the sliding sediments has low shear strength and high velocity, the inertial component is significant (Dutta and Hawlader 2018). In these cases, fluid mechanics approach is more appropriate to model the impact of debris flow

or turbidity current (Zakeri et al. 2008, 2009). Randloph and White (2012) proposed a hybrid method for estimation of drag force, combining the geotechnical and fluid mechanics approaches. Previous studies related to lateral pipe–soil interaction can be categorized into three classes: (i) theoretical and analytical approaches, (ii) physical modelling, and (iii) numerical modelling.

### 2.3.1 Theoretical and analytical approaches

Demars (1978) studied the pipeline failures those took place in the Gulf of Mexico during 1971–1975 and proposed an analytical approach to estimate the tension induced in a pipeline subjected to submarine landslide impact. In this analysis, it was assumed that pipelines subjected to landslide behaves similar to a cable suspending a load on it. The shear forces and bending moments in the pipeline were ignored for simplicity. It was concluded from the analysis that pipelines experience greatest amount of tension when landslides occur in the direction parallel to the pipeline axis and the least when it is perpendicular. Following formulae were proposed to estimate the drag force on the pipelines:

$$F_{D,90} = N_c \times s_u \times D \tag{2.3}$$

$$F_{D,0(max)} = F_{D,90} \times f \tag{2.4}$$

where, $F_{D,90}$ is component of drag force perpendicular to the pipeline axis; $F_{D,0(max)}$ is the maximum value of drag force component parallel to the pipeline axis; $N_c$ is the bearing capacity factor and $f$ is the geometric tension factor. $f$ can be determined from Fig. 2.3 using the inputs: initial angle between the pipeline axis and seabed contour, $\theta$; deflection angle (measured with respect to the pipeline axis), $\alpha$; length of pipeline segment affected by landslide, $L$, and elongation of the pipeline, $\Delta L$.

The effects of mudslide impact on the pipelines in the Mississippi delta were studied by Swanson and Jones (1982). They also supported the opinion of Demars (1978) and stated that the primary cause of pipeline failure is the tensile force built in the pipeline during the mudslide impact. They recommended a constant value for *k* parameter and proposed a simplified mathematical model to estimate the drag force on buried pipelines through following formulae:

$$F_{D,90} = 10 \times s_u \times D \tag{2.5}$$

$$F_{D,0} = \pi \times s_u \times D \tag{2.6}$$

In this mathematical model, slide angle was measured relative to the pipeline axis, axial and transverse soil resistances as well as bending stiffness and pipeline curvature effects were considered. It was concluded that pipeline burial and smaller pipe diameters reduce the risk of failure; whereas, high operation pressure and thick coating increase the risk of failure during the landslide impacts. Finally, they stated that likelihood of survival of pipeline is the least when slide occurs is the direction parallel to the pipeline axis and the greatest when normal to the pipeline axis. The oversimplified analyses of Demars (1978) led them erroneously to opposite conclusions.

Summers and Nyman (1985) also studied the mudslide effects on buried pipelines analytically considering the geometrical nonlinearities of pipeline (large displacement), nonlinear soil resistance (anchorage in no-slide zone) and nonlinear behavior of pipe material. They adopted the principle of virtual work to calculate the stresses and strain induced in the buried pipeline and presented following simplified mathematical equations for estimating the drag forces (parallel and perpendicular to the pipeline axis) within and outside the slide zone:

$$F_{D,0(max)} = \alpha \times s_u \times \pi \times D \tag{2.7}$$

$$F_{D,90(max)} = N_{ch} \times s_u \times D \tag{2.8}$$

where, $\alpha$ is the adhesion factor (to be determined using Fig. 2.4(a)); and $N_{ch}$ is the bearing capacity factor (to be determined using Fig. 2.4(b)).

### 2.3.2 Physical modelling

Lateral pipe–soil interaction was also investigated through physical modelling—small-scale testing, flume experiments, and centrifuge testing (Brookes and Whitmore 1968; Paulin et al. 1995, 1998; Phillips et al. 2004; Oliveira et al. 2009; Zakeri et al. 2008; Chi 2012; Sahdi et al. 2014). Most of these studies were conducted either on buried pipelines or partially embedded pipelines; except Zakeri et al. (2008) and Chi (2012), who focused on suspended or free-spanning pipes.

Zakeri et al. (2008) performed a series of laboratory flume tests with kaolin clay slurry to study the impact of clay-rich debris on both surface-laid and suspended pipelines. They adopted the fluid mechanics approach and proposed a method to estimate the drag force normal to the pipeline axis caused by submarine debris flow impact. The experiments were carried out in a 10 m long, 3 m high and 0.6 m wide tank. The slurry was prepared mixing kaolin clay, silica sand, black diamond coal slag and water; the concentration of slurry was varied by varying the quantities of kaolin clay and silica sand. The rheology of the slurry was modeled using the Power-law and Herschel-Bulkley (non-Newtonian) fluid models. They modified the definition of Reynold's number for non-Newtonian fluids (Eq. 2.10) and defined the drag coefficient, $C_D$ using Eq. (2.2).

$$\mathrm{Re}_{\mathrm{Newtonian}} = \frac{\rho \times U_\infty^2}{\mu \times \dot{\gamma}} \tag{2.9}$$

$$\mathrm{Re}_{\mathrm{non-Newtonian}} = \frac{\rho \times U_\infty^2}{\mu_{\mathrm{app}} \times \dot{\gamma}} = \frac{\rho \times U_\infty^2}{\tau} \tag{2.10}$$

$$C_D = \frac{F_D}{\frac{1}{2} \times \rho \times U_\infty^2} \tag{2.11}$$

where, $\rho$ is the density of the flow, $U_\infty$ is the velocity, $\mu$ is the absolute (dynamic) viscosity, and $\mu_{app}$ is the apparent viscosity (defined as the ratio of fluid shear stress, $\tau$ and strain rate, $\dot{\gamma}$). They established a relationship between the non-Newtonian Reynold's number and coefficient of drag force (Fig. 2.5) and proposed an equation (Eq. 2.12) to estimate the drag force on suspended pipelines.

$$C_D = 1.4 + \frac{17.5}{\mathrm{Re}_{\text{non-Newtonian}}^{1.25}} \tag{2.12}$$

Their study showed that with the increase of clay percentage in the slurry, the drag coefficient increases, which eventually increases the drag force on the pipeline. Flow separation regions were observed for slurries containing more than 30% clay (Fig. 2.6). As the shear strength of debris increases (i.e., clay percentage of slurry increases), this flow separation results in the formation of a closed channel behind the pipe and entraps free-water (completely different from pore-water) in that channel. The entrapped free-water creates a suction that causes an additional component to the drag force on the suspended pipes (Dutta and Hawlader, 2018; Saha et al. 2018).

Chi (2012) presented a centrifuge modelling technique to model the impact of a sliding glide block on a suspended pipeline. He adopted the conventional geotechnical approach to estimate the drag force. A total of 11 set of experiments were performed under the submerged condition in a geotechnical centrifuge at a centrifugal acceleration of 30g (i.e. $N$ = 30), where g is the gravitational acceleration. The pipeline was placed at the mid-height of the 4.5-m high (prototype height) kaolin clay blocks. The undrained shear strength of the clay blocks was varied between 4 and 8 kPa, and the impact velocities ranged between 0.04 to 1.3 m/s. Analyzing the results of 11 tests, the $k$ parameter of Eq. 2.1 was found to be a function of the shear strain rate, $\dot{\gamma}$ (Fig. 2.7) and expressed the relation in terms of the following power-law relationship:

$$k = F_D/s_u D \ = 7.5 \times \dot{\gamma}^{0.12} \quad (2.13)$$

This study concluded that the drag force on pipeline also depends on the shear strain rate ($\dot{\gamma}$) in addition to the undrained shear strength of the impacting clay block and pipe diameter. Though this study provided with a quick and efficient method of estimating drag force, there was no mention of the effect of burial depth and the gap between a suspended pipeline and seabed ($g$). Note that some studies on the effect of gap ratio ($\hat{g} = g/D$) on the hydrodynamic forces on the pipeline are available in the literature (Roshko et al. 1975; Goktun 1975; Bearman and Zdravkovich 1978; Lei et al. 1999; Yang et al. 2008). Experimental evidence showed that the drag coefficient, $C_D$ strongly depends on the gap ratio, $\hat{g}$—a circular cylinder experiences the lowest drag force when it lies on the plane boundary (e.g. seabed), i.e. at $\hat{g}$ = 0 because of maximum pressure on the seabed at this situation. As $\hat{g}$ increases, the base pressure decreases, and $C_D$ increases gradually. The drag coefficient, $C_D$ becomes stable when $\hat{g} \geq 1.5$. The effect of gap ratio on the drag coefficient is shown in Fig. 2.8.

### 2.3.3 Numerical modelling

Because of the substantial time and cost associated with physical tests, and taking the advantages of modern computational advancements, the application of numerical analysis (e.g., Finite Element (FE) analysis, Computational Fluid Dynamics (CFD) analysis) of lateral pipe–soil interaction has become popular recently. Advanced numerical techniques have been developed in the last few decades that can model pipe–soil interaction more accurately considering many important features. Moreover, numerical simulations being inexpensive and less time consuming, can be used over and over again at will, to model various scenarios to cover a wide range of parametric study. In the literature, a large number of numerical studies are available on pipelines subjected to lateral loading. Generally, a section of pipeline is modelled (mostly as a rigid body) in a domain of soil

and dragged laterally by using displacement or velocity boundary condition (Paulin et al.1998; Popescu et al. 2002; Phillips et al. 2004, Dutta et al. 2014). Another approach is to keep the pipe section fixed at its position and allow the soil mass (debris or block) slide laterally and impact the pipe (Zakeri et al. 2009a; Zhu and Randolph, 2009; Zakeri et al. 2013; Dutta and Hawlader, 2015, 2018; Saha et al. 2018). For modelling large deformation scenario, Hu and Randolph (1988a, b) developed a two-dimensional LDFE technique using re-meshing and interpolation with small strain (RITSS) approach which is based on conventional small-strain FE formulation embedded with automatic remeshing and interpolation of stress parameter and field materials. A number of researchers have used this technique for modelling the large deformation phenomena—for example, Zhu and Randolph (2009) used the similar scheme to model submarine landslide impact on partially to fully embedded (embedment ratio ranging from 0.005 to 3.0) pipelines. They showed that seabed strength influences the process of engulfment of pipe and can play a significant role on the drag force generated on the pipeline during the debris flow impacts (as shown in Fig. 2.9). They also illustrated that when the debris strength is sufficiently higher than the seabed strength, the debris materials erode the seabed and fully engulf the partially embedded pipeline. However, they modelled the soil as an elastic-perfectly plastic material, i.e. strain-softening and strain rate effects were not considered. The effect of free-water suction was also ignored which could play a significant role in the estimation of drag force on the pipeline.

Zakeri (2009) developed a computational fluid dynamics approach to estimate the normal and longitudinal drag forces on suspended pipelines based on the laboratory flume tests conducted by Zakeri et al. (2008). The numerical results matched with the test results satisfactorily and provided a means to investigate the effect of other factors controlling the drag force. In this study, he demonstrated the effects of debris strength and impact velocity on the drag force. He stated that

the normal drag force on the pipe is a result of viscous force and dynamic pressure; whereas, longitudinal drag force is due to the shear stress developed around the pipe surface. For design purposes, he proposed the following two equations to estimate the drag coefficients:

$$C_{D\_90} = 1.4 + \frac{17.5}{\mathrm{Re}_{\text{non-Newtonian}}^{1.25}} \tag{2.14}$$

$$C_{D\_0} = 0.08 + \frac{9.2}{\mathrm{Re}_{\text{non-Newtonian}}^{1.1}} \tag{2.15}$$

Randolph and White (2012) reanalyzed the test data of Zakeri et al. (2008) and developed a hybrid approach combining the geotechnical and fluid mechanics approach to quantify the drag force on the pipeline. Martin and White (2012) developed another numerical technique to estimate the ultimate bearing capacity of a 'wished in place' pipe using OxLim (a finite element software developed at Oxford University) which is based on the limit equilibrium theorem. The model pipe was dragged vertically and laterally to estimate the penetration, uplift and lateral resistances. This study provided with a guideline to estimate the undrained capacity of a pipe for a wide range of soil type ($\gamma' D/s_u$ = 0, 1, 3, 5 or $\gamma' z/ s_u$ = 0, 1, 3, 5, where z is the depth below mudline), pipe–soil interface conditions (full tension/no tension, smooth/rough) and embedment ratios. Finally, a set of *V–H* failure envelopes for different scenarios were proposed which can be used to estimate the lateral resistance in various conditions. Dutta and Hawlader (2018) conducted a numerical investigation using CFD approach to estimate the drag force on suspended pipelines considering the strain-rate and strain-softening effects of clay. They modeled the debris as a non-Newtonian fluid using dynamic viscosity and forced the material to flow to impact a suspended pipe. The limitations of predefined pipe–soil interface condition (full tension/no tension or smooth/rough) in the region of water entrapment was eradicated as their model could successfully simulate the

development of suction (i.e. tensile force on pipe) in that zone. They mentioned that a large penetration distance is needed to mobilize the maximum drag force, and this drag force is primarily dominated by the geotechnical resistance of the debris flow at lower Reynolds number (Re < 0.5) but inertial component becomes significant in case of higher Reynolds number (Fig. 2.10). They proposed a set of equations to estimate the drag force on suspended pipelines. However, they did not consider the effect of the gap between the pipe and seabed, though this gap can play a major role in case of fluid flow around a cylindrical pipe (Roshko et al. 1975; Geöktun, 1975; Bearman and Zdravkovich, 1978; Lei et al. 1999; Yang et al. 2008). Yang et al. (2008) investigated the effect of gap on hydrodynamic force on pipelines and seabed for unidirectional ocean current. They showed that as the gap between the pipeline and seabed increases, the drag coefficient, $C_D$ increases, whereas the lift coefficient, $C_L$ decreases gradually (Fig. 2.11). Both the drag coefficient and lift coefficient reach a stable value as the gap ratio is greater than 1.

This literature review insinuates that approaches for quantifying the drag force on suspended pipelines during the submarine landslides have been developed progressively over the last few decades, but still there is significant room for improvement and new research by incorporating the missing segments into the current work.

## 2.4 Summary

This chapter presents the previous studies on lateral pipe–soil interaction during submarine landslides. The prevailing state-of-the-art includes experimental, analytical and numerical techniques of quantifying the drag force. The effects of the seabed strength and the gap between the pipeline and seabed are the two issues that need to be investigated properly. To investigate the effects of these two factors, large deformation finite element (Abaqus CEL) and finite volume (Ansys CFX) software packages have been used in the present study.

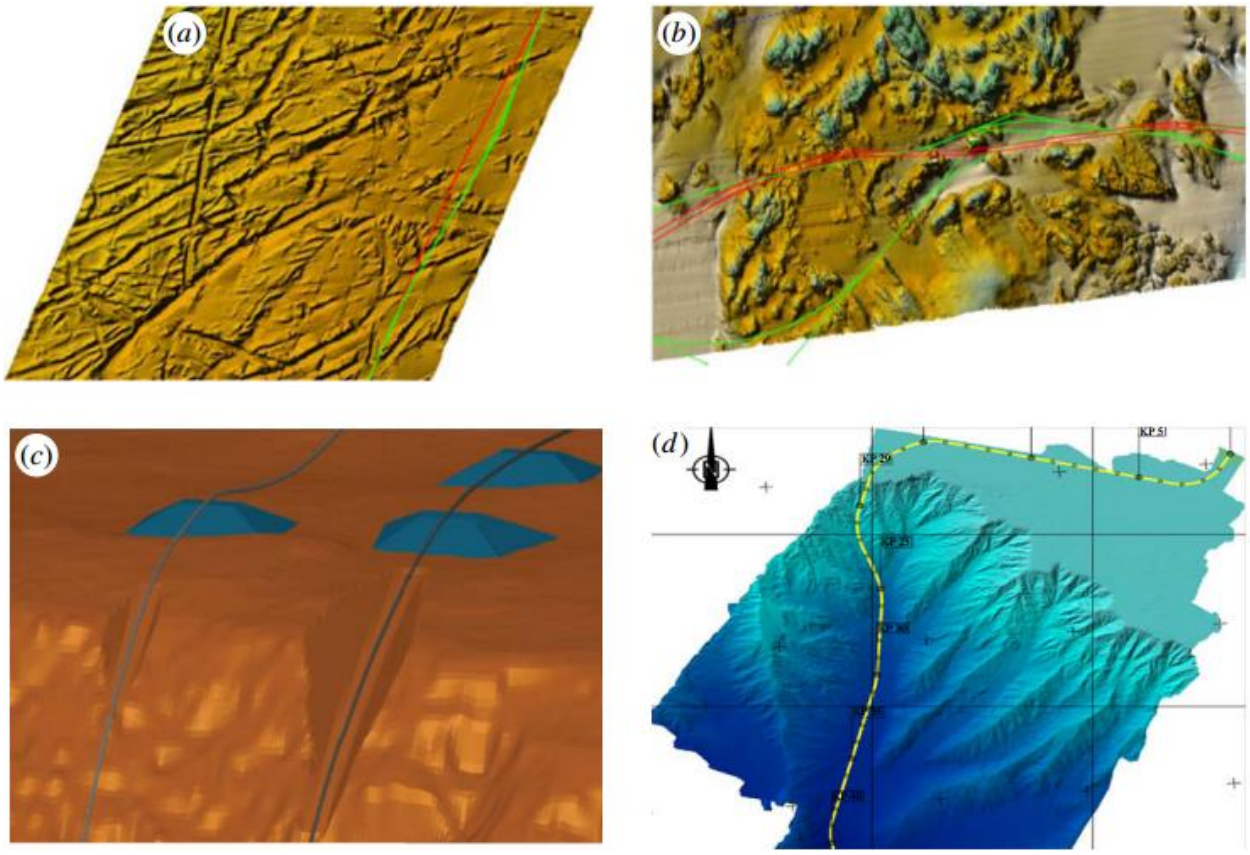


**Figure 2.1.** Occurrence of free-spanning of offshore pipelines: pipelines passing through (a) rough zone caused by iceberg scars, (b) soft clayey sediment and rock outcrops, (c) sharp shelf break and (d) rough continental slope (after Drago et al. 2015)

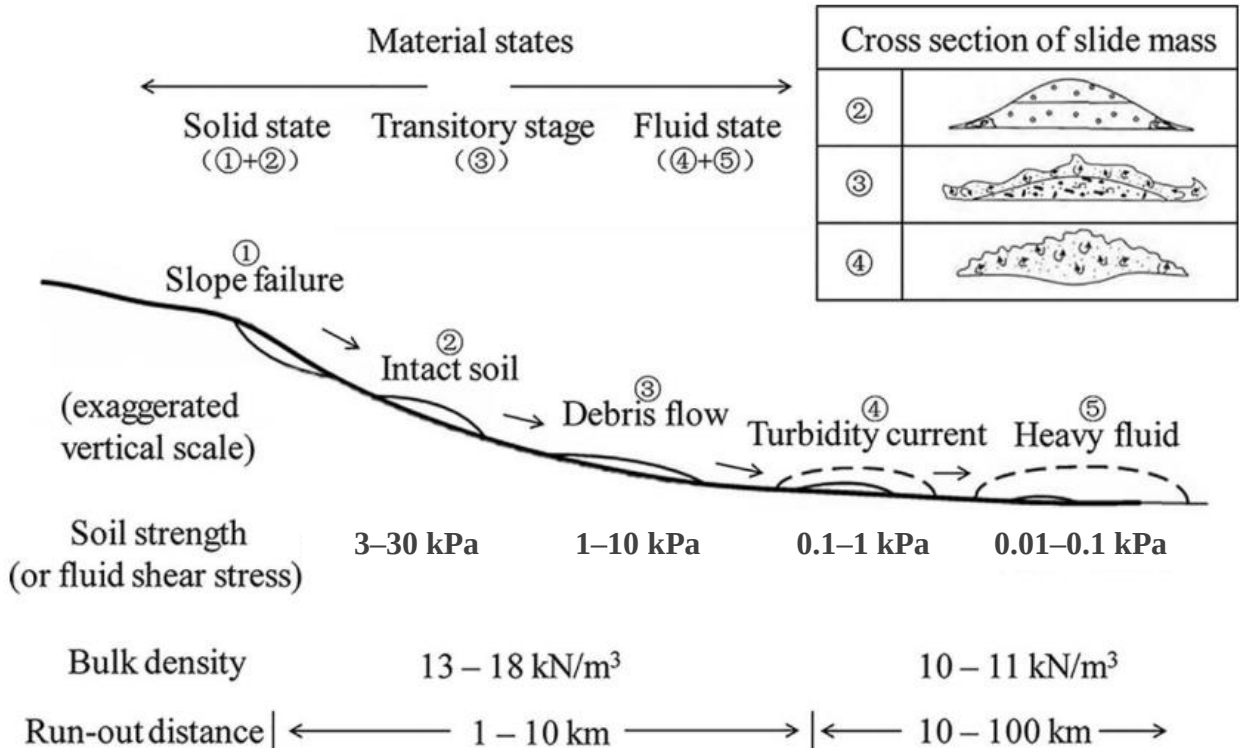


**Figure 2.2.** Phases of submarine landslides (after Fan et al. 2017)

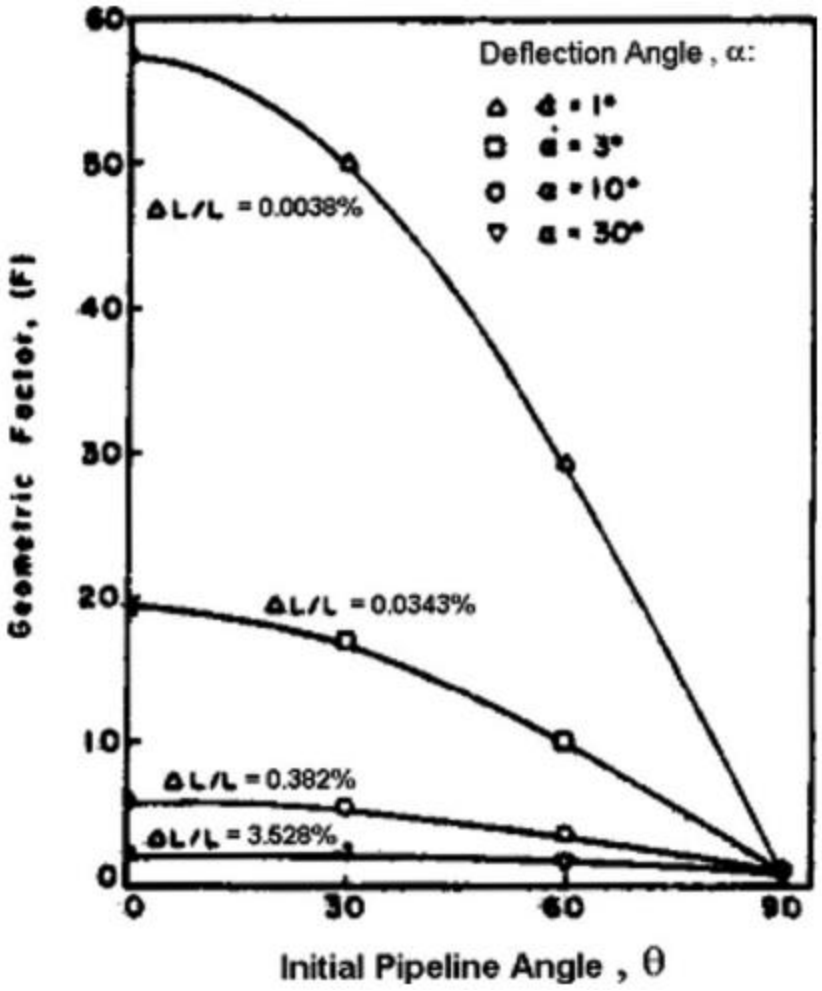


**Figure 2.3.** Determination of geometric factor, *f* (Demars 1978)

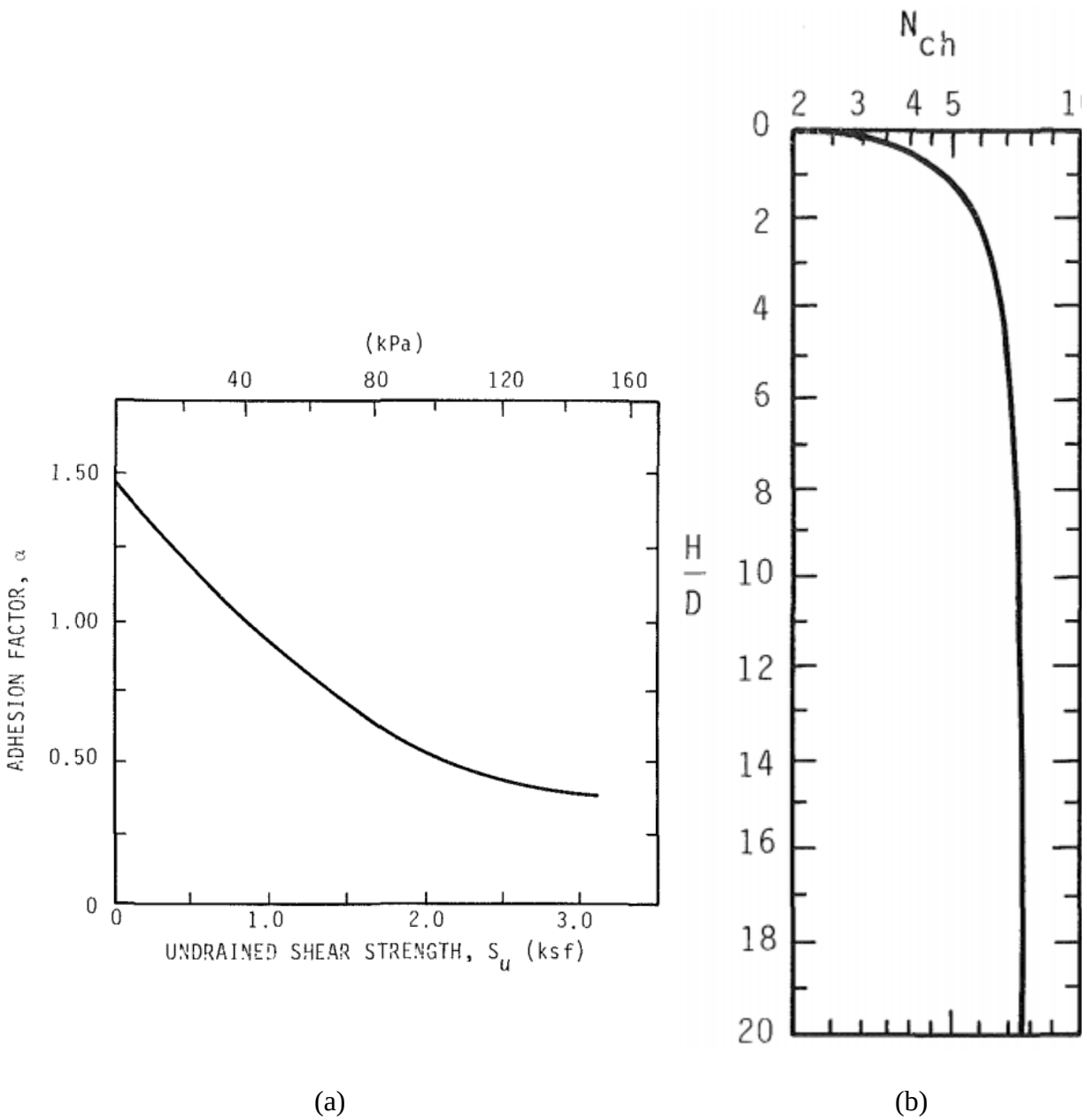


(a) (b)

**Figure 2.4.** Estimation of drag force using Summer and Nyman's equation: (a) adhesion factor–undrained shear strength curve; (b) horizontal bearing capacity–burial depth ratio curve (after guidelines for the seismic design of oil and gas pipeline systems, NY 1984)

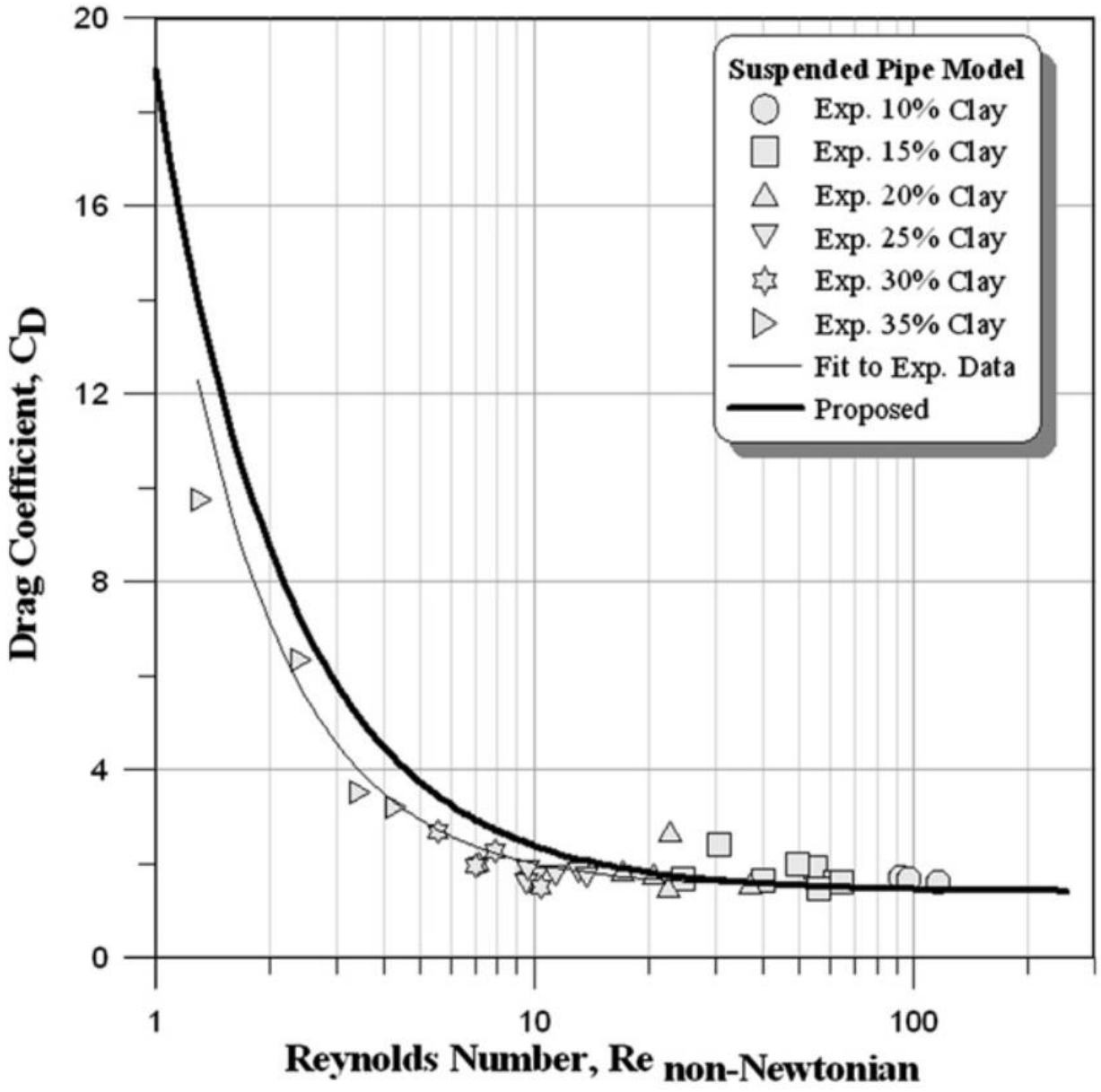


**Figure 2.5.** Drag coefficient versus Reynolds number for suspended pipe (after Zakeri et al. 2008)

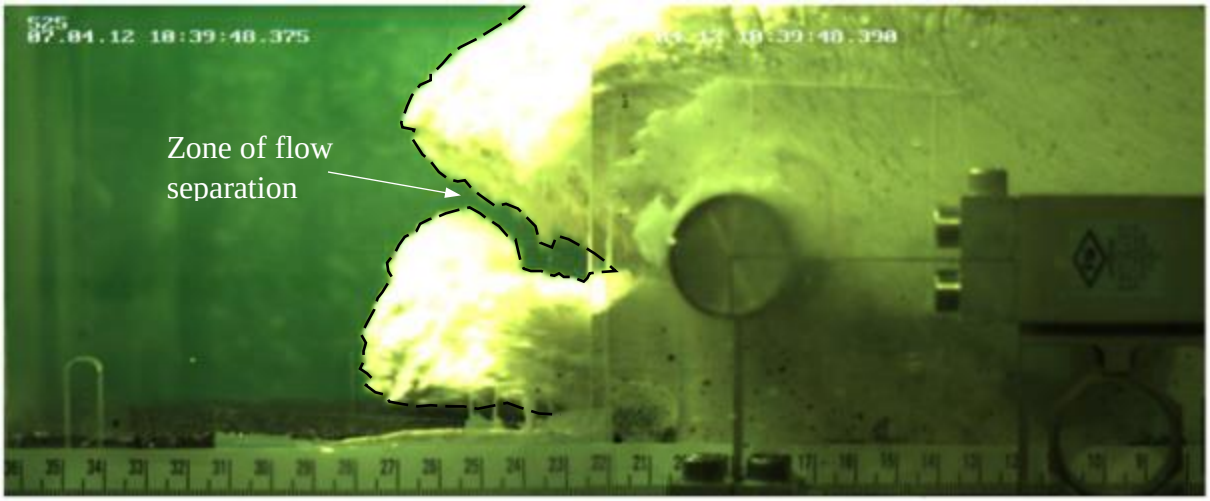


**Figure 2.6.** Flow separation during the impact on a suspended pipeline (Zakeri et al. 2008)

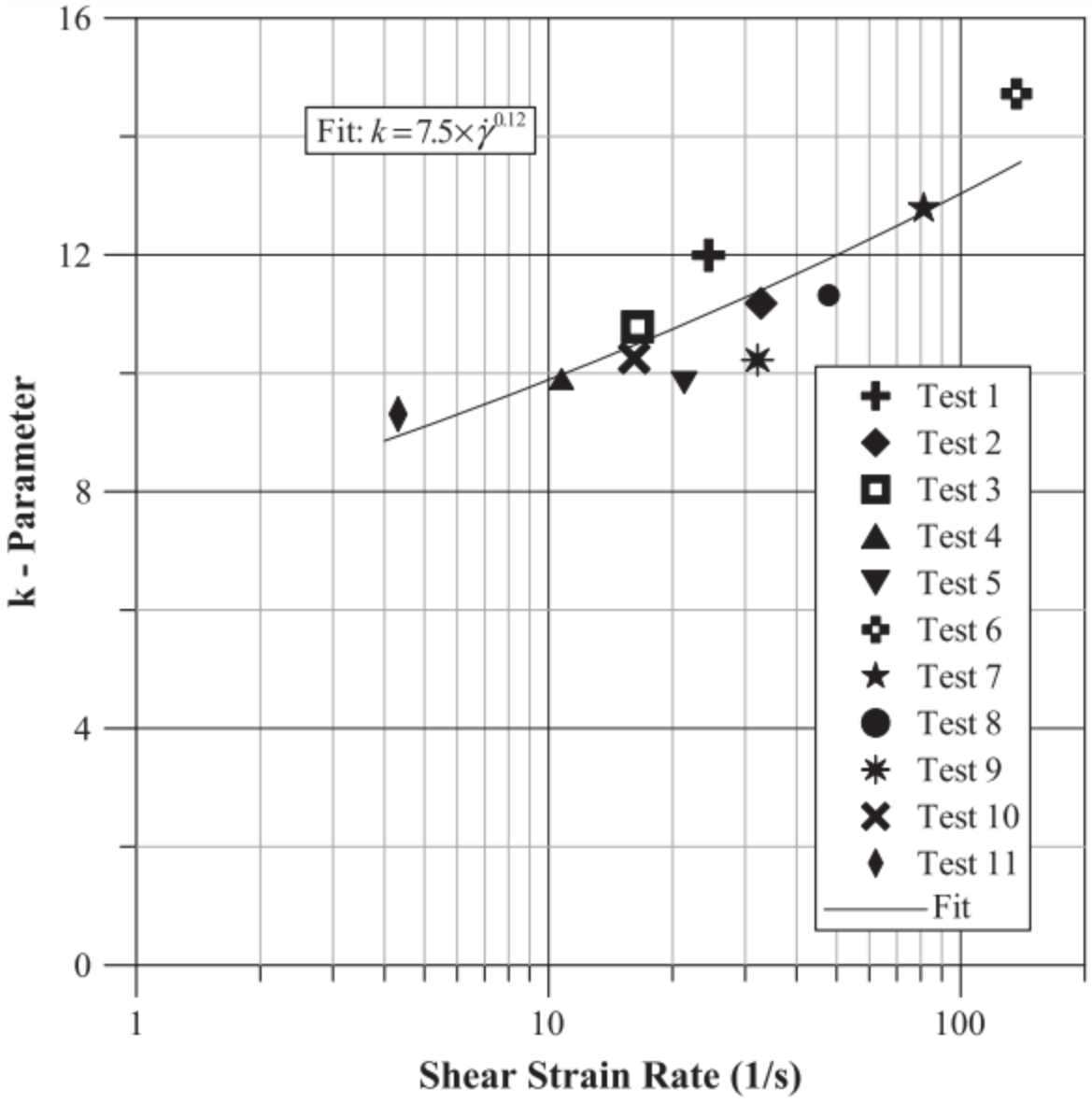


**Figure 2.7.** *k*-parameter versus shear strain rate, $\dot{\gamma}$ (after Zakeri et al. 2012)

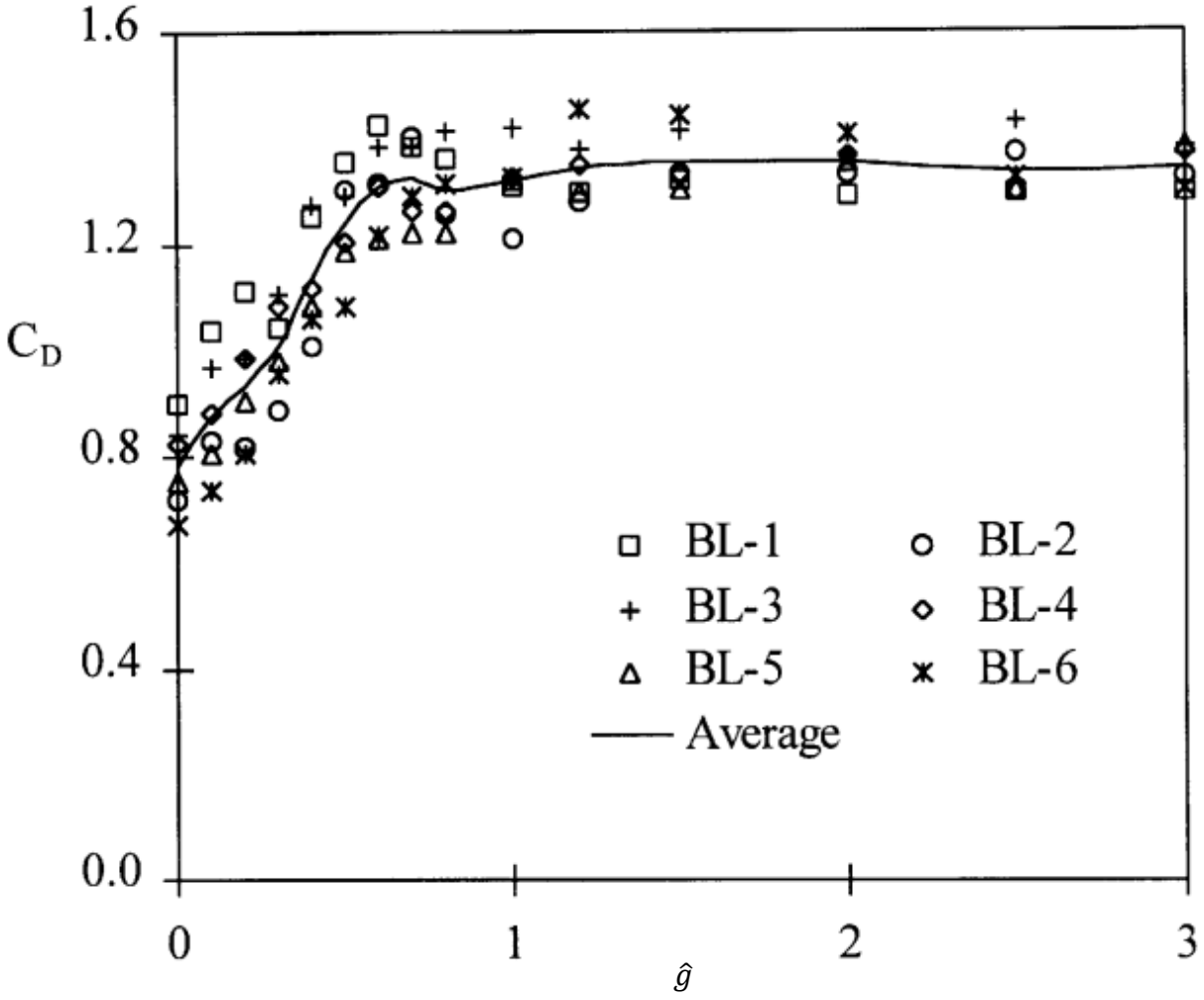


**Figure 2 8.** Drag coefficient, $C_D$ versus gap ratio, $\hat{g}$ (after Lei et al. 1998)

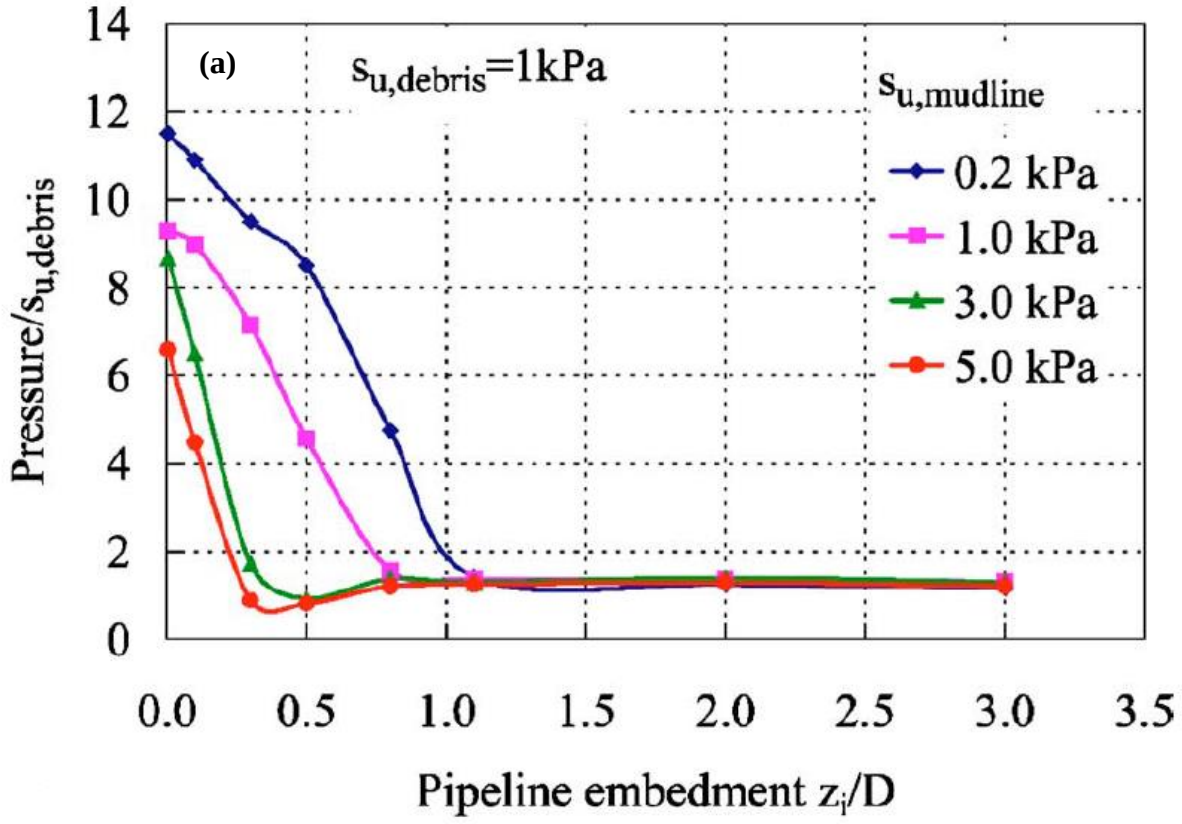
(a)
$s_{u,debris}$=1kPa
$s_{u,mudline}$
0.2 kPa
1.0 kPa
3.0 kPa
5.0 kPa
Pressure/$s_{u,debris}$
Pipeline embedment $z_i$/D
0
2
4
6
8
10
12
14
0.0
0.5
1.0
1.5
2.0
2.5
3.0
3.5

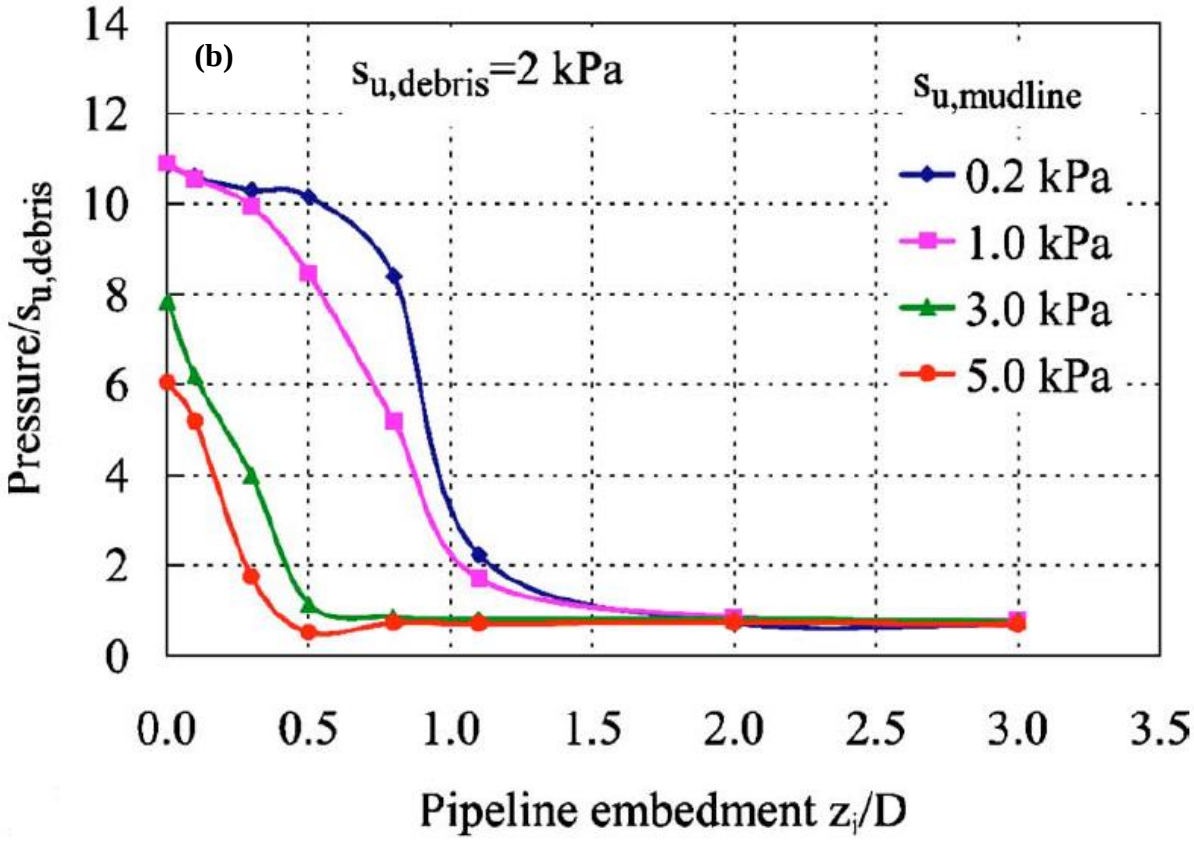
(b)
$s_{u,debris}$=2 kPa
$s_{u,mudline}$
0.2 kPa
1.0 kPa
3.0 kPa
5.0 kPa
Pressure/$s_{u,debris}$
Pipeline embedment $z_i$/D
0
2
4
6
8
10
12
14
0.0
0.5
1.0
1.5
2.0
2.5
3.0
3.5

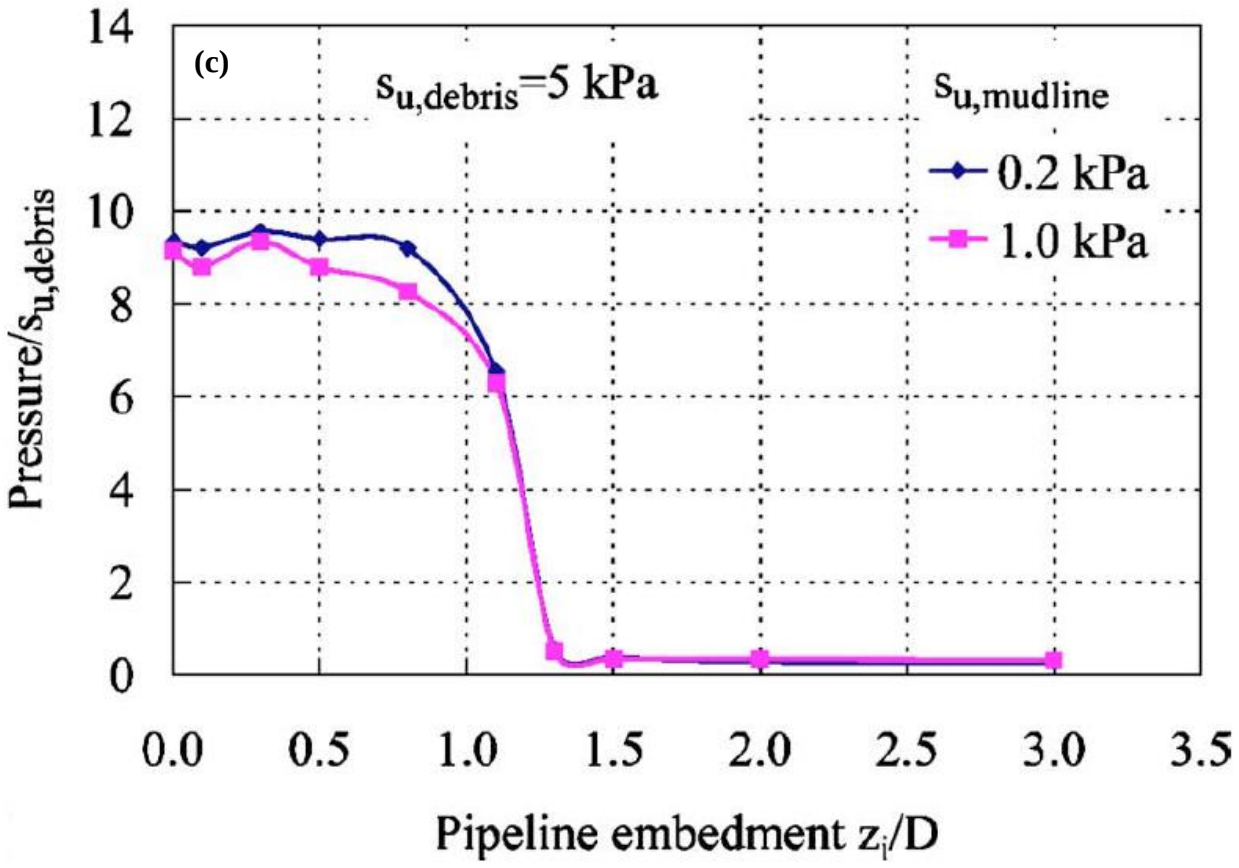


**Figure 2.9.** Variation of pressure on pipeline for different seabed strengths and debris strengths (after Zhu and Randolph, 2012)

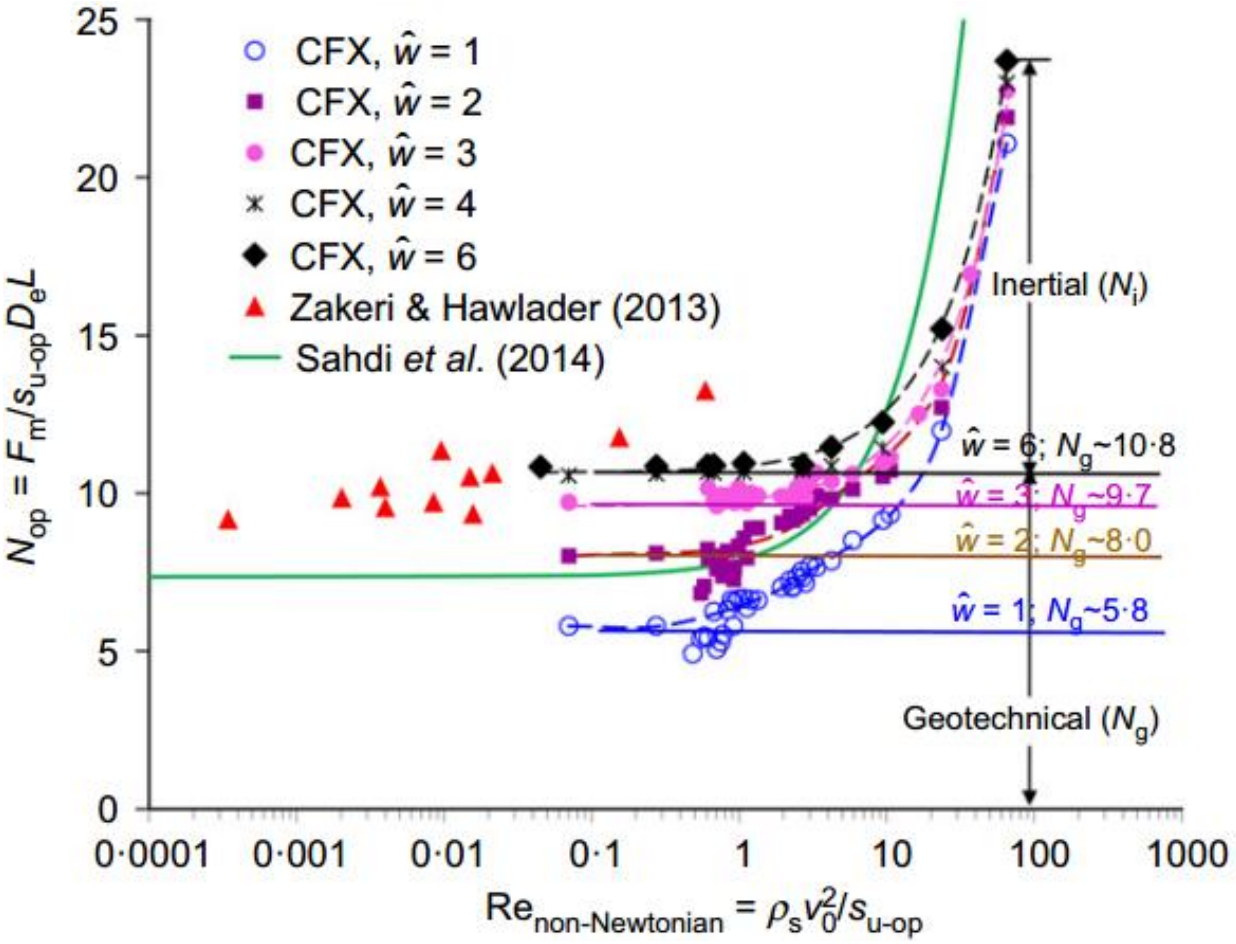


**Figure 2.10.** Maximum normalized drag force versus non-Newtonian Reynolds number (after Dutta and Hawlader, 2018)

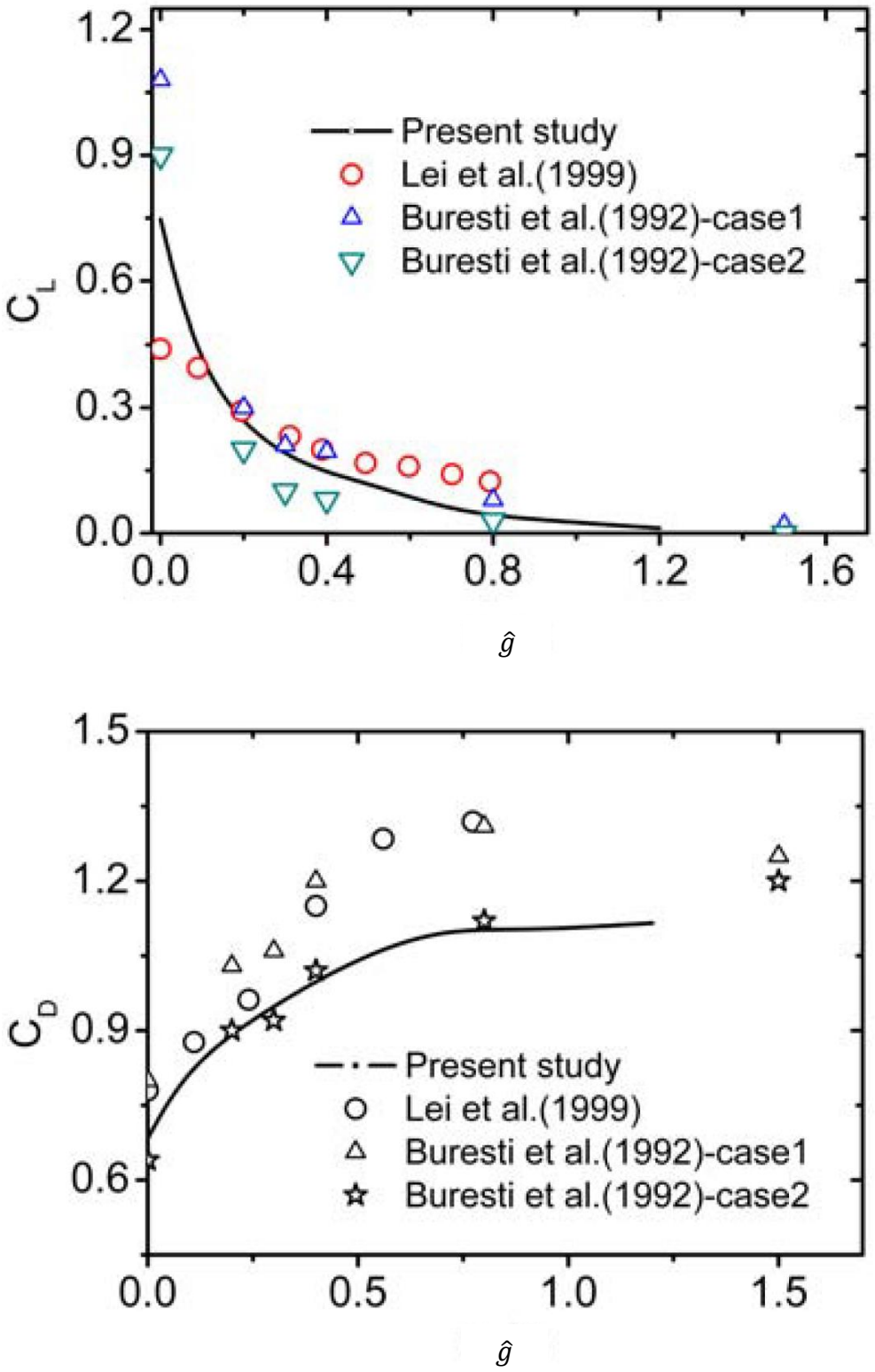


**Figure 2.11.** Variation of lift coefficient, $C_L$ and drag coefficient, $C_D$ with gap ratio, $\hat{g}$ (after Yang et al. 2008)

# Chapter 3

# Performance Evaluation of Finite Element and Finite Volume Software Packages in Modelling Pipe–Soil–Water Interaction

## 3.1 General

Offshore pipelines play an effective and efficient role in transporting hydrocarbons (oil and gas) from the offshore production facility to the onshore receiving terminal. Generally, offshore pipelines are laid in a trench and backfilled with soil to prevent mechanical damages due to extensive trawling and assure on-bottom stability. But in deepwater environments (depth >400 m), they are often laid on the seafloor as trenching in that condition is very challenging. When a pipeline is laid on an uneven seabed, a section of the pipeline might be suspended between two high points. This suspended pipeline might be affected by a failed seabed sediment that originates from the submarine landslides those frequently occur in offshore environment. When a failed soil mass strikes a suspended pipeline, a complex pipe–soil–water interaction takes place. In present study, both Finite Element (ABAQUS) and Finite Volume (ANSYS CFX) software packages have been used for numerical modelling of this pipe–soil–water interaction and the more computationally efficient software package is used for further study.

## 3.2 Introduction

Many small to large-scale landslides occur in offshore environments. A failed soil mass that generates from a submarine landslide might travel a large distance over the seafloor. Generally, offshore slopes are mild; a typical slope angle is less than 10°, except for some locally steep slope areas (Hadj-Hamou and Kavazanjian 1985, Dey et al. 2016). One of the major submarine landslides in Canadian history is the Grand Banks landslide of 1929, which involved transportation

of 100–150 $km^3$ of sediments and damaged several transatlantic telegraph cables that were located hundreds of kilometers downslope from the place where the failure was initiated (Piper et al. 1988, 1999, Fine et al. 2005). The occurrence of many other submarine landslides has been reported in the literature (Piper et al. 1988, 1999, Bondevik et al. 2005, De Blasio et al. 2005, Masson et al. 2006).

Offshore pipelines are generally laid on the seafloor in deepwater environments (depth >400 m) and might penetrate into the soft clay seabed because of their weight, installation and hydrodynamic effects. When a pipeline is laid on an uneven seabed, a section of the pipeline might be suspended between two high points. A suspended pipeline might be affected by a failed seabed sediment that originates from a submarine landslide.

Arnold (1967) reported that, out of the 271 pipeline failures in the Mississippi delta during 1958–1965, approximately 55% of the pipeline failures were due to soil movements. Demar et al. (1977) showed that ~20% of the 125 pipeline failures in the Gulf of Mexico from 1971 to 1975 were also caused by soil movement. Therefore, proper estimation of pipeline drag force resulting from soil movement is one of the design requirements for offshore pipeline design.

The present study focuses on modelling the impact force of debris flow originating from a submarine landslide on a suspended pipeline. Experimental, analytical and numerical studies were conducted in the past for an estimation of drag force. The experimental works include small-scale laboratory tests and centrifuge tests, where a relative displacement between a section of pipe and surrounding soil was applied and the resistance of the soil was measured (Paulin et al., 1998; Phillips et al., 2004; Sahdi et al. 2014). Zakeri et al. (2009) conducted a series of flume tests to study the impact of clay-rich debris on suspended pipelines. Chi (2012) conducted centrifuge tests

where a glide block struck on a pipeline perpendicular to its direction of movement, at a wide range of impact velocities.

Zakeri (2009c) summarized various approaches commonly used to estimate drag force on pipelines or piles. Two approaches are used to calculate the drag force: a geotechnical approach and a fluid mechanics approach. In the geotechnical approach, the drag force is proportional to the undrained shear strength ($s_u$) of the sliding clay block (e.g., Summers and Nyman 1985; Georgiadis 1991; Zhu and Randolph 2009). In the fluid mechanics approach, the soft debris is considered as a fluid and the drag force is proportional to the square of the impact velocity (Jiang and LeBlond 1993; Zakeri et al. 2008). Randloph and White (2012) proposed a combined geotechnical and fluid mechanics approach. The inertial component of drag force becomes significant when the impact velocity is high and/or debris shear strength is low (Sahdi et al. 2014; Dutta and Hawlader 2018).

Two types of numerical approaches could be used to calculate drag force: (i) large deformation finite element analysis and (ii) computational fluid dynamics approach. To determine the impact of a clay-rich debris on a suspended pipeline, two important numerical issues need to be resolved. First, what will be the interface behaviour as the debris engulfs the pipe which was initially surrounded by water? Second, when the debris flows around the pipe, a cavity forms behind it; whether this cavity has an influence on the drag force or the pipeline–soil interface behaviour can be simply modelled as bonded (full-tension)/unbonded (no-tension) and smooth/rough interface conditions, as commonly used in FE analysis. In the present study, these issues will be studied through numerical simulation of submarine landslide impacts on suspended pipelines, using a large deformation finite element modelling technique and a computational fluid dynamic approach.

## 3.3 Problem Statement

Figure 3.1 schematically shows three stages of the process of impact. A block of failed soil mass displaces in the downslope direction at a velocity *v* over the seabed (Fig. 3.1a). When it impacts a pipeline on its way, depending upon the location with respect to the seabed, the soil in the block might be displaced around the pipeline, as shown in Fig. 3.1(b). At this moment, the front part of the pipe is in contact with the soil. The force exerted by the failed soil mass is primarily due to penetration resistance, which is controlled by soil strength. Note that if the impact velocity is high, the inertial component also plays a significant role in the drag force (Sahdi et al. 2014; Dutta and Hawlader 2018). With a further displacement of the failed soil mass, the debris engulfs the pipe (Fig. 3.1(c)). However, a cavity behind the pipe will be formed, which might be connected to free water, and will be completely closed after a large displacement of the debris. The suction in the water-filled cavity would play a major role in the drag force (Dutta and Hawlader 2018).

## 3.4 Numerical modelling

### 3.4.1 Finite Element modelling

The coupled Eulerian-Lagrangian approach available in Abaqus FE software is used for large deformation FE modelling. The details of numerical modelling, including its advantages and limitations, have been discussed in previous studies (Wang et al. 2015; Dutta et al. 2015). The size of the Eulerian domain (abcd in Fig. 3.2) is 4.35 m × 2.9 m (width × height). The seabed below this domain is considered as a rigid body. As the pipe is far from the seabed, the drag force will not be influenced by seabed behaviour. The soil is modelled as a Eulerian material. Since the Eulerian analysis allows only three-dimensional modelling, all the analyses are performed for a one-element thickness of 14.5 mm of the domain in the out-of-plane direction (i.e. along the axial

direction of the pipe) to replicate a plane strain condition. The FE model comprises five parts: pipe, soil, water, void and seabed (Fig. 3.2).

The FE domain is discretized using EC3D8R elements in Abaqus, which is an 8-noded hexahedral linear brick, reduced integration Eulerian element with hourglass control. Fine mesh is used near the pipe. The thickness of the elements is ~15 mm near the pipe, which is increased to 29 mm at a distance of five times of the diameter from the centre of the pipe, as shown in Fig. 3.3(a). Cubical elements of 29-mm length are used outside this zone.

The soil is modelled as elastic–perfectly plastic material, by defining the von Mises yield strength ($= 2s_u$), where $s_u$ is the undrained shear strength.

The free water is also modelled as a Eulerian material using a hydrodynamic material model by defining it in the form of the Mie-Grüneisen equation of state, which is available in Abaqus as a built-in model. Soil and free water are assigned in the domain by using the Eulerian Volume Fraction (EVF) tool—EVF equals 1 for Eulerian materials and 0 for the void.

Generally, in pipeline–soil interaction modelling, the pipeline is modelled as a Lagrangian body together with an appropriate contact definition for the interface. The currently available versions of Abaqus cannot simulate the bonding between the pipeline and surrounding soil/water, using full-tension interface conditions. However, bonding plays a significant role in drag force (Dutta and Hawlader 2018). The present study uses the following approach to simulate a fully bonded condition.

Instead of defining the pipe as a Lagrangian body, the pipe section (a circular hole of void) is extruded from the Eulerian body. The pipe surface is defined using a set of nodes on the wall. During the analysis, the velocity of these nodes is set to zero ($v_x = v_y = v_z = 0$); therefore, no

Eulerian material can enter in the pipe—that is, the pipe surface behaves as an impermeable wall. Summing up the x-component of the nodal force of the nodes along the circumference of the pipe, the force on the pipe ($F_x$) is calculated.

The left and right boundaries of the domain are defined as an inlet and outlet, respectively. At the outlet, in addition to the velocity boundary condition, an equilibrium outflow boundary condition is used. This ensures the reduction of spurious reflection of the Eulerian materials at the outflow boundary. This boundary condition is used because the pressure distribution is unknown. A free-slip boundary condition is used for the interface between the seabed and debris/free water. All the out-of-plane vertical surfaces are assigned with a $v_y = 0$ boundary condition.

The numerical analysis is divided into two steps: gravitational loading and debris flow. In the first step, the gravity is applied gradually to achieve the in-situ stress condition of the soil and hydrostatic stress condition in the free water. In the second step, the debris block is forced to slide laterally to the right by applying a velocity boundary condition in the x-direction ($v_0 = 0.2$ m/s) at the inlet and outlet.

### 3.4.2 Finite Volume modelling

ANSYS CFX software is used for the computational fluid dynamics analyses. The geometry and boundary conditions in CFX analysis are the same as for Abaqus CEL modelling, as discussed above. However, no void space is required above the water, as in CEL modelling, as shown in Fig. 3.3(b). The pipe is modelled as a wall with a no-slip boundary condition. Clay and water are modelled as multiphase homogenous Eulerian materials.

The shear resistance of clay is defined using the dynamic viscosity, $\mu_d$ (= $s_u/\dot{\gamma}$, where $\dot{\gamma}$ is the shear strain rate), as a rigid-plastic non-Newtonian fluid. A constant dynamic viscosity of $8.9\times10^{-7}$ kPa.s is used for water. Further details of CFX modelling are discussed in chapter 4.

## 3.5 Parameter selection

Table 3.1 summarizes the geometry and properties of clay and water used in this study. For FE analysis, the clay is modelled as an elastic-perfectly plastic material with an undrained Young's modulus of $500s_u$. Although the undrained shear strength of debris can vary with depth, it is assumed to be uniform ($s_u$ = 5 kPa). Moreover, the effects of strain rate and strain softening on $s_u$ are not considered in this study.

## 3.6 Results

### 3.6.1 Force–displacement behaviour

Figure 3.4 shows the normalized force ($N_h = F_x/s_{uN}D_eL$) versus normalized lateral penetration ($\hat{u} = u/D_e$) curves obtained for FE and CFX simulations. Here, $s_{uN} = 2/\sqrt{3}s_u$, $L$ = length of the pipe in the out-of-plane direction, $D_e = D_o + t_i$, where $t_i$ is the average thickness of the soil elements just outside the pipe surface (Hawlader et al. 2015, Dutta and Hawlader 2018). The lateral penetration distance at time $t$ is calculated as $u = v_0(t-t_0)$, where $t_0$ is the time when the pipe touches the sloped surface and the force on the pipe starts to increase.

Figure 3.4 shows that $N$ increases rapidly with $\hat{u}$ up to $\hat{u} \sim 2$; thereafter, the rate of increase of $N$ is small. At $\hat{u}$ between 4 and 5, the normalized resistance is almost constant. (For points A, B, C, D see Fig. 3.5.) In both CFX and CEL analyses, the resistance again increases after $\hat{u} \sim 5$, which is because of the development of suction in the cavity that forms behind the pipe, as discussed in

the following sections. For the analyses performed in this study, both CFX and CEL give similar force–displacement curves.

### 3.6.2 Soil failure mechanisms

Figure 3.5 shows the development of plastic shear strains ($\gamma_p = \int_0^t \dot{\gamma}\, dt$) in the soil for different levels of penetration, as shown by open squares and triangles in Fig. 3.4. Dutta et al. (2015) and Dutta and Hawlader (2018) provided the details on plastic shear strain calculation, which is used in the current study. At 1.3*D* penetration, the plastic shear strain is mainly accumulated in front of the pipe (left side) (Figs. 3.5(a) and 3.5(b)). At 5*D* penetration, a considerable heave occurs above the pipe together with a large shear strain accumulation (Figs. 3.5(c) and 3.5(d)). At this time, a wide channel is formed behind the pipe (right side), which is filled with free water. As the channel is wide, free water can flow easily through it; therefore, the free water does not have any significant effect on the lateral force, and the force at this stage is primarily governed by the geotechnical resistance of clay. Some difference between soil failure and accumulated plastic shear strain obtained from CEL and CFX is potentially due to the difference in solution techniques used in these software packages for modelling of sediment. With an increase in penetration, the channel becomes smaller and, at $\hat{u} \sim 6$–7, it is almost closed in both CFX and CEL simulations (Figs. 3.5(e) & 3.5(f)). The length of closure increases with further penetration, and the cavity behind the pipe becomes almost isolated from the free water at $\hat{u} > 10$ ((Figs. 3.5(g) & 3.5(h)). When the channel becomes narrow or closes, a suction (i.e. total pressure is below the initial ambient pressure) generates in the water in the cavity, which influences the lateral resistance, as discussed in the following sections.

### 3.6.3 Role of water in the channel/cavity behind the pipe

The suction behind the pipe for two large penetration distances is shown in Fig. 3.6. In CFX, the pressure ($p$) is obtained for each time increment. The zone of water where $p$ is less than the initial ambient pressure (defined as a reference pressure in the analysis) represents the area where suction is developed. In CEL, the initial ambient pressure is calculated at each location after the gravity step, which is defined as a state variable. Using a user subroutine, the suction is calculated by subtracting the initial ambient pressure from the current pressure. Note here that the negative pressure in the soil (outside the dashed line that represents the water-filled cavity in Fig. 3.6), can be viewed as the tension in soil elements.

Comparison between suction contours in Fig. 3.6 shows that, although the magnitude of suction is comparable in CEL and CFX simulations, there is a difference between the shape and size of the zone where suction is developed. This is primarily due to the modelling technique and especially the modelling of the soil–water interface. Because of this, the size/shape of the water-filled cavity is different, as shown in Fig. 3.5. However, as the magnitude of suction is comparable, the force–displacement curves are similar, as shown in Fig. 3.4.

In pipeline–soil interaction modelling—for example, vertical and lateral resistance calculations—free water is not modelled explicitly as a separate phase. Instead, the soil is modelled using the submerged unit weight ($\gamma'$) and pipe–soil interface is considered as having smooth/rough and fully-bonded/unbonded conditions (e.g. Martin and White 2012; Dutta et al. 2015). To show the advantages of free water modelling and effects of bonding, the following three sets of FE analyses are performed, and the results compared with previous analyses. In Case-I, FE analysis is performed with a void only (instead of water as in Fig. 3.2) and $\gamma'$ as the unit weight of the soil block. The fully bonded condition, as described above, is used. In Case-II, the pipe is modelled as

a Lagrangian body where interface behaviour is defined as a smooth and rough condition, without bonding, while the other conditions are the same as in Case-I. The Case-III analyses are performed using Abaqus/Explicit for a wished-in-place pipe configuration for fully-bonded and unbonded together with smooth and rough interface conditions. In all three cases, air (void) was considered in place of water. The force–displacement curve for Case-I only is shown by blue dotted line in Fig. 3.4. For the other cases, the calculated maximum force is shown in Table 3.2. Table 3.2 shows that the maximum normalized force for the unbonded cases is significantly lower than for the bonded cases. As expected, the lowest force is calculated with an unbonded and smooth pipeline–soil interface condition. The bonded behaviour could not be simulated properly in CEL without modelling free water explicitly; therefore, Case-I simulation gives a significantly lower maximum force than that obtained in presence of water (as shown in Fig. 3.4). For the cases analyzed in this study, the maximum force for Case-III with a fully bonded and rough interface condition is comparable to that in Fig. 3.4. Note, however, that the Case-III analyses are for a wished-in-place pipe configuration where a relatively small displacement is required to reach the maximum force, and the role of cavity and surface heave, as shown in Fig. 3.5, on drag force, is not modelled. Maximum normalized force of 6.40 is estimated using American Lifelines Alliance (ALA) and Pipeline Research Council International (PRCI) guidelines, which shows a close agreement with the unbonded cases. But higher maximum normalized values than the guidelines are observed for fully bonded cases where soil/water/pipe interaction is considered.

### 3.6.4 Computational cost

Like other large deformation finite element analyses, Abaqus CEL is computationally expensive. The CEL analysis presented in Fig. 3.4 took 51.5 hours with a Core™ i7-6700 CPU @ 3.40 GHz, 16.0 GB RAM desktop. For the same computer, the CFX analysis in Fig. 3.4 took only 5 hours. In

other words, the modelling of a submarine landslide's impact on pipeline using ANSYS CFX is computationally efficient compared to Abaqus CEL analysis.

## 3.7 Conclusions

Deepwater offshore pipelines are generally laid on the seafloor and can be either partially embedded or suspended. Suspended pipelines might interact with a submarine landslide-induced failed soil mass that can damage the pipeline. Proper estimation of pipe drag force is an important design parameter, which depends on many factors, including impact velocity, shear strength debris, pipeline–soil interface behaviour and free water. Dutta and Hawlader (2018) modelled this process, including the role of free water, using a computational fluid dynamics (CFD) approach. In the present study, it is shown that the coupled Eulerian-Lagrangian (CEL) approach of finite element analysis can be used to model this process. However, in CEL, free water and interface behaviour (e.g. bonding) should be modelled properly. Although the force–displacement behaviour obtained from CFD and CEL are comparable, the CFD modelling using ANSYS CFX is computationally efficient. For further study, ANSYS CFX will be used.

The simulations are performed for ideal soil (without considering strain rate and softening effects on undrained shear strength) and only one burial depth, pipe diameter and impact velocity. Further studies are required to investigate the effect of these parameters on drag force.

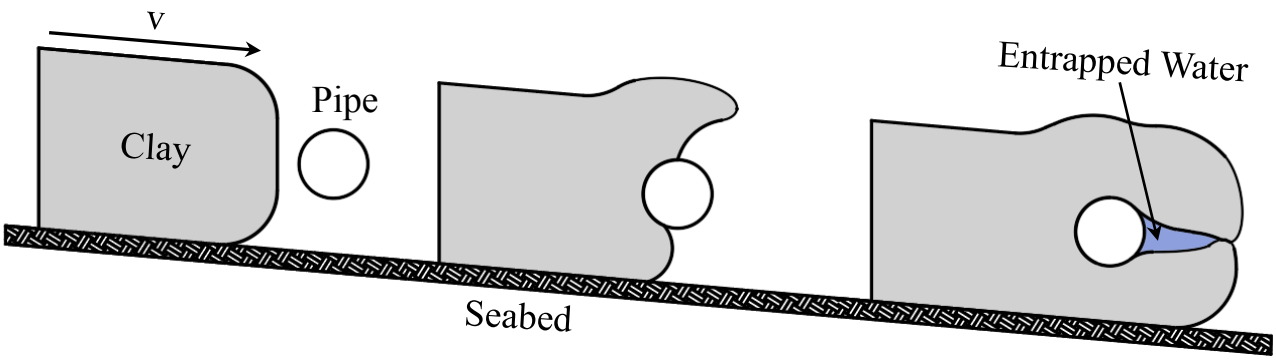


(a) Stage 1 (b) Stage 2 (c) Stage 3

**Figure 3.1.** Stages of submarine landslide impact on suspended pipelines

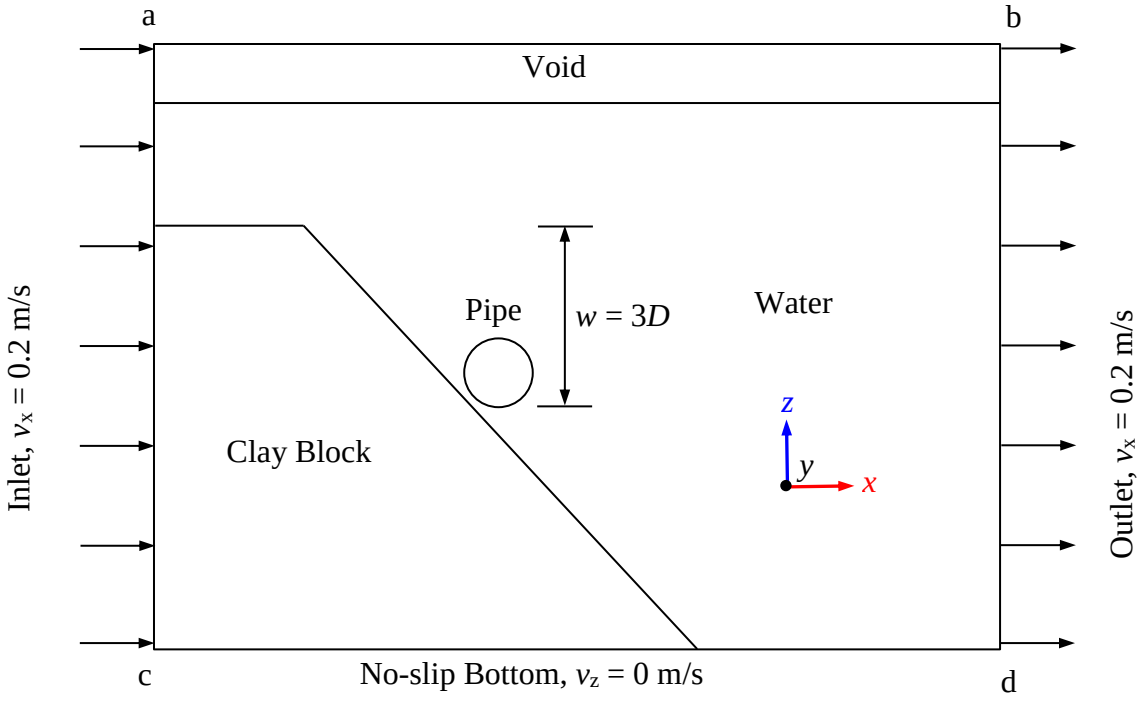


**Figure 3.2.** Details of FE modelling

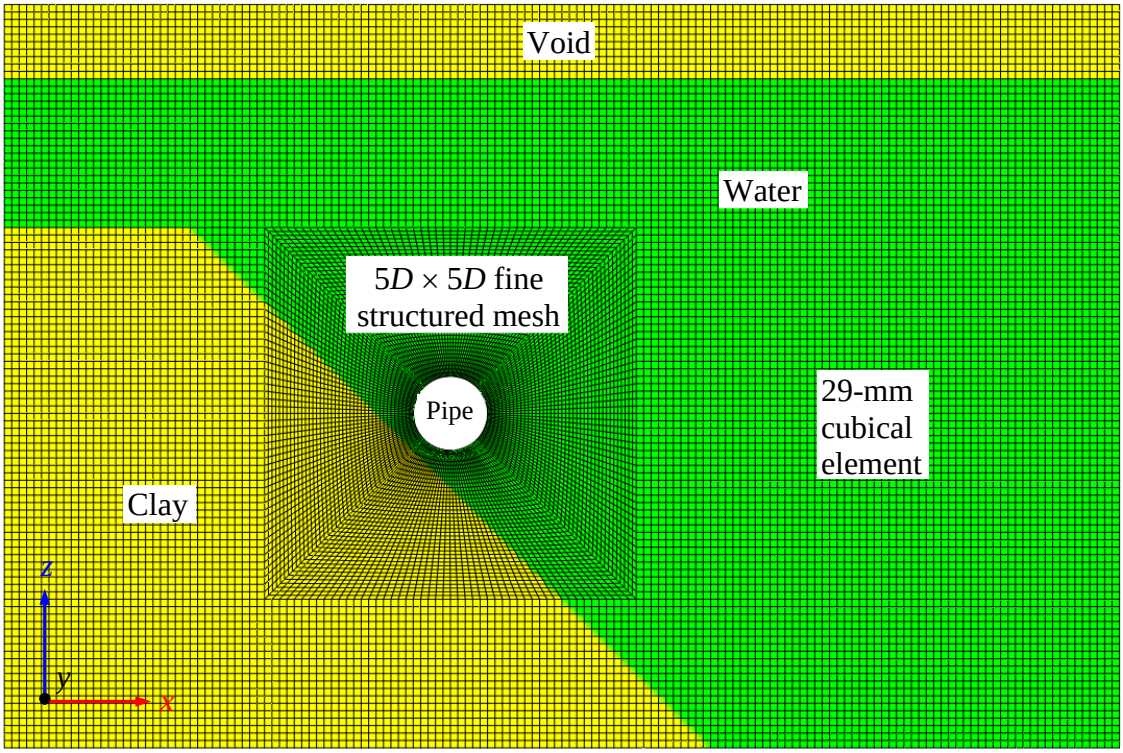


(a)

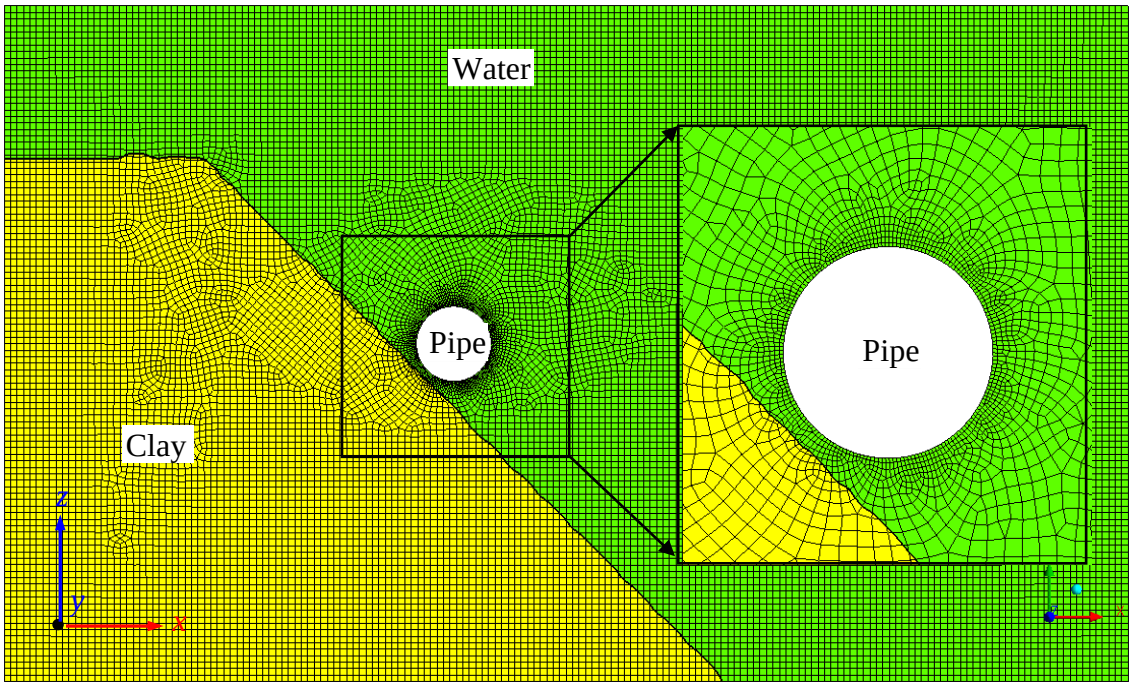


(b)

**Figure 3.3.** Mesh around the pipe: (a) Abaqus (b) ANSYS CFX

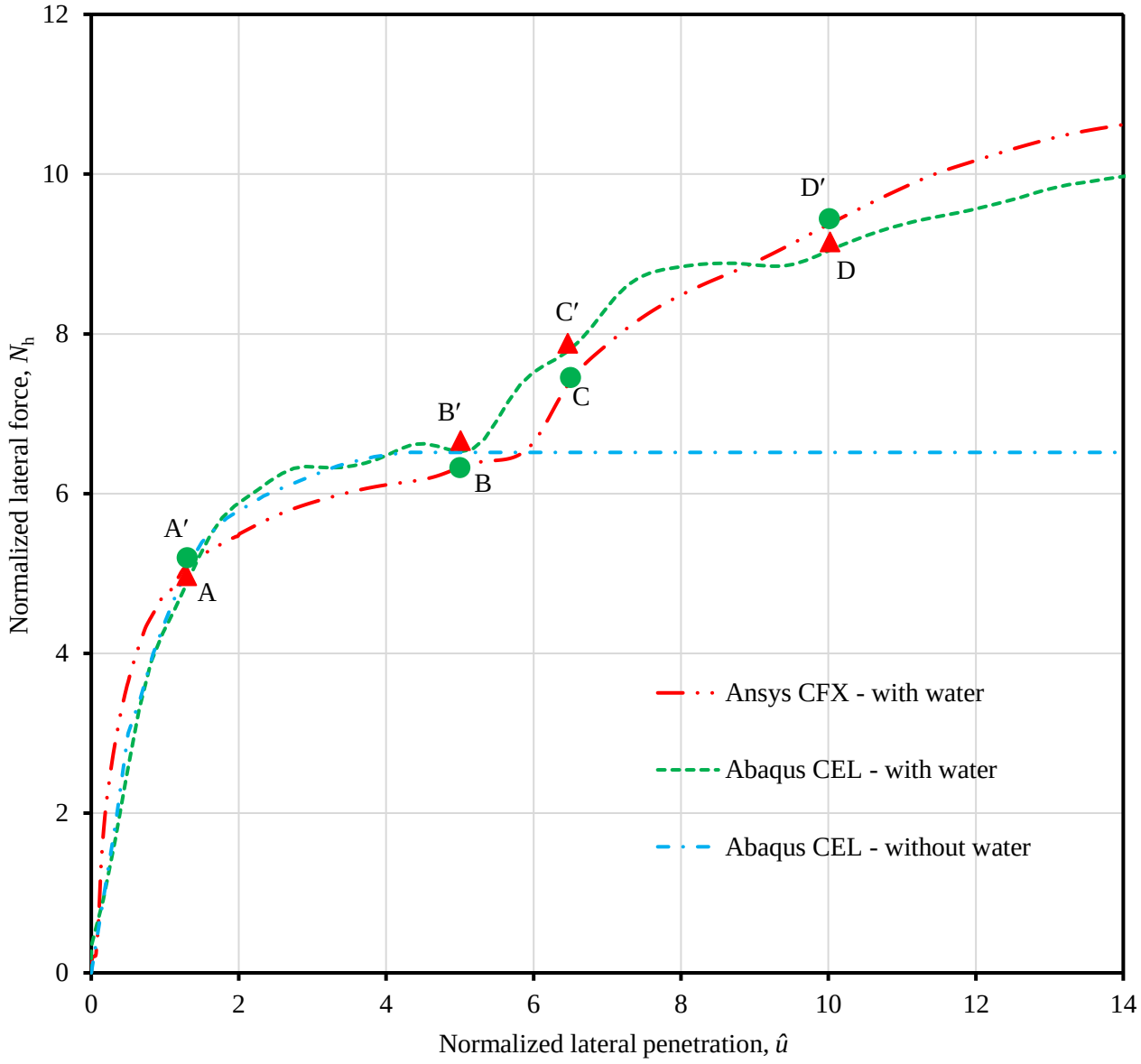


**Figure 3.4.** Normalized force–displacement curves

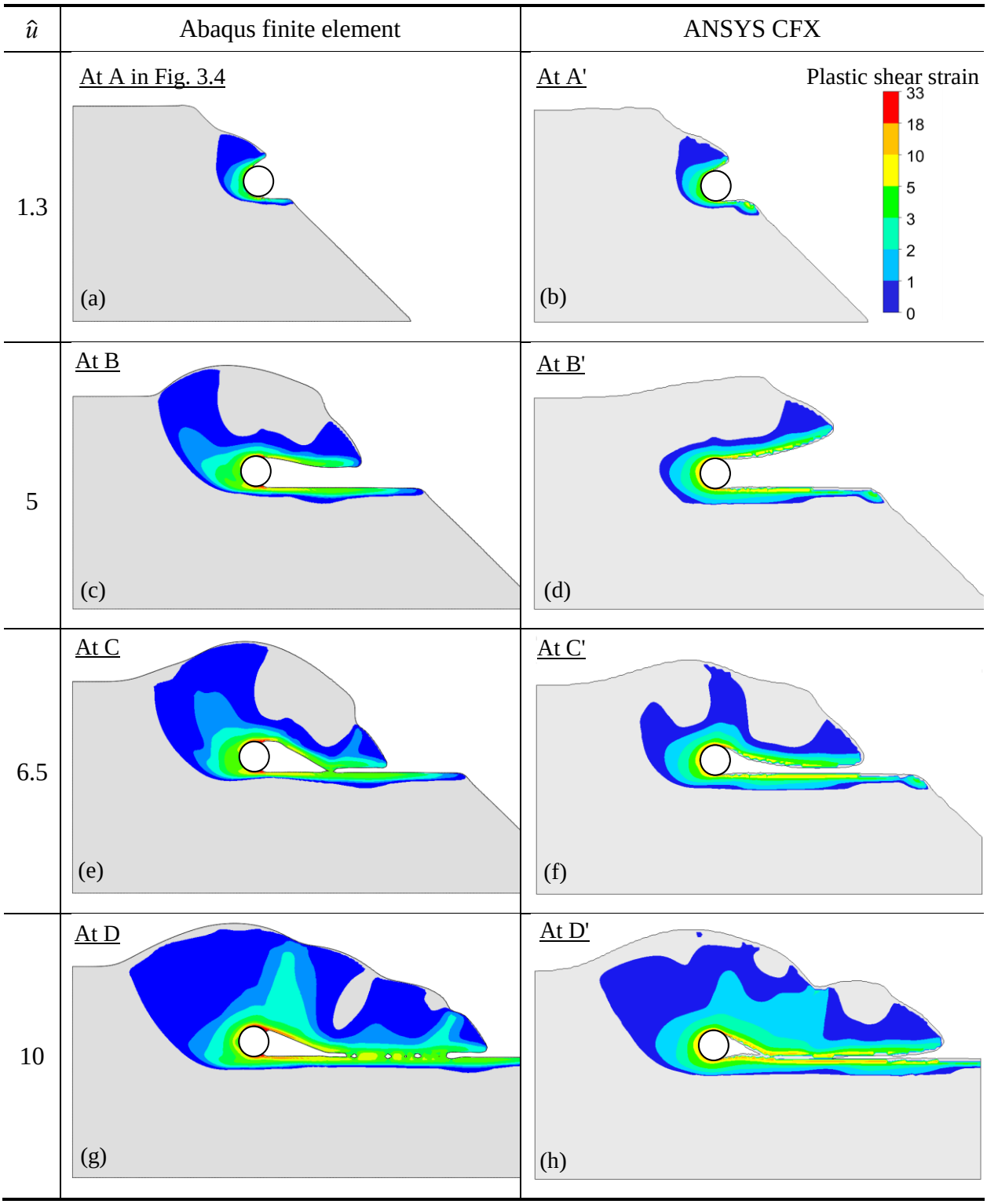


**Figure 3.5.** Development of plastic shear strain, $\gamma_p$ and soil failure with pipe penetration

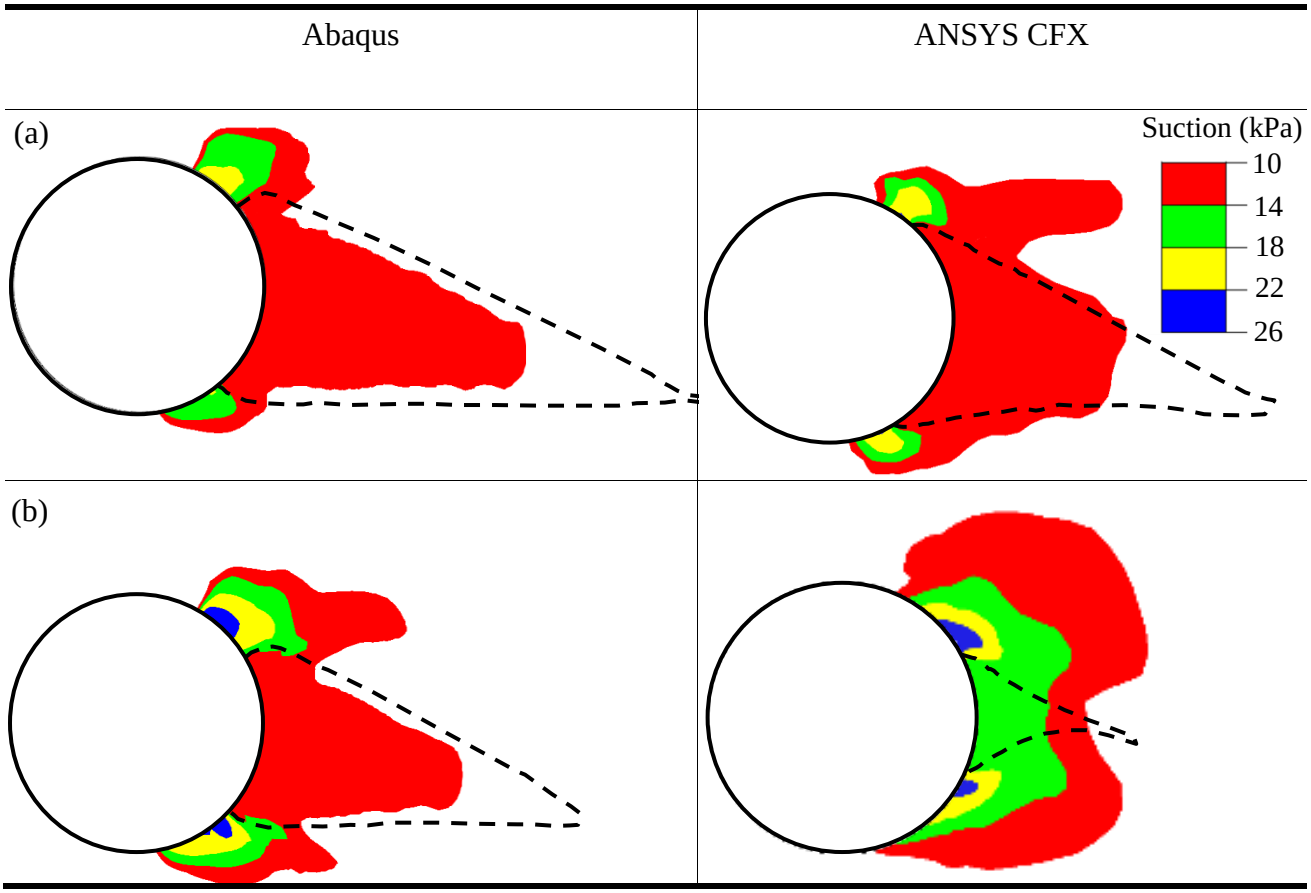


**Figure 3.6.** Comparison of suction around the pipe in Abaqus and Ansys CFX at: (a) $u = 10D$; (b) $u = 14D$

**Table 3.1.** Parameters used in numerical analysis

| | |
|---|---|
| **Pipe:** | |
| Outer diameter, $D_o$ | 290 mm |
| Length, $L$ | 14.5 mm |
| **Clay:** | |
| Undrained shear strength, $s_u$ | 5 kPa |
| Undrained Young's modulus in FE analysis, $E_u$ | $500s_u$ |
| Undrained Poisson's ratio in FE analysis, $\nu_u$ | 0.495 |
| Saturated unit weight of soil, $\gamma_{sat}$ | 15.81 kN/m$^3$ |
| **Water:** | |
| Equation of State (EOS) | |
| Velocity of sound in water, $c_0$ | 1531 m/s |
| Slope of $U_s - U_p$ curve, $s$ | 0 |
| Grüneisen ratio, $\Gamma_0$ | 0 |
| Dynamic viscosity of water in CFX and FE analysis, $\mu_D$ | $8.9 \times 10^{-7}$ kPa.s |
| Unit weight of water, $\gamma_w$ | 9.81 kN/m$^3$ |

**Table 3.2.** Maximum normalized resistance for different interface conditions

| Case No. | Interface behaviour | | Maximum horizontal normalized force, $N_{h(max)}$ |
|---|---|---|---|
| Case-I | - | Full tension | 6.5 |
| Case-II | Smooth | No tension | 5.2 |
| | Rough | No tension | 5.9 |
| Case-III | Smooth | Full tension | 9.2 |
| | Rough | Full tension | 10.8 |
| | Smooth | No tension | 5.75 |
| | Rough | No tension | 6.5 |

# Chapter 4

# Effects of Seabed Shear Strength and Gap between Pipeline and Seabed on Drag Force on Suspended Pipelines Caused by Submarine Debris Flow

## 4.1 General

As-laid pipelines in offshore environments might be suspended at a varying distance above the seabed, depending upon the seabed undulations. During the process of run-out of a sliding soil mass/debris, resulting from a submarine landslide, the debris might impact these pipelines. When impacted, the pipeline might interact with not only the debris but also the seabed soil, depending upon the gap between pipeline and seabed. A proper quantification of the drag force resulting from submarine landslides is required in the design of a pipeline to avoid its damage and ensure serviceability. Previous studies show that a number of factors affect the drag force, including the debris strength, diameter of the pipe, velocity of the sliding mass, and depth of embedment when the debris engulfs the pipe. The present study investigates the effects of undrained shear strength of the debris and underlying seabed and the gap between the pipeline and seabed (suspended pipes) on drag force, in addition to the aforementioned factors.

## 4.2 Introduction

Pipelines are one of the most reliable components of offshore hydrocarbon transportation system to transport oil and gas in shallow to deep water environments. In deep water, due to high installation cost, pipelines are often laid on the seafloor instead of burring them through trenching and backfilling. Due to the unevenness of topology of seabed and scouring effects, some segments of the pipe may be hanging between two high points, which results in a free-spanning scenario. Sometimes, the pipelines might pass through the mudslide or landslide prone areas. Moreover, the

failed soil mass originated from the landslide might traverse several hundred kilometers (Kvalsad et al. 2001) and impact the pipelines. For example, the Grand Banks landslide in 1929 involved downslope movement of 100–150 $km^3$ sediments that damaged telecommunication cables and other seafloor installations, located several hundred kilometers away from the location of initiation of the landslide (Piper et al. 1988, 1999; Fine et al. 2005).

Lateral pipe–soil interaction during submarine landslides has been studied by a number of researchers. These studies can be categorized into three groups: (i) theoretical or analytical approach, (ii) physical modelling, and (iii) numerical approach. Analytical approaches and mathematical models to quantify pipeline stresses and drag force on pipelines impacted by submarine landslides have been proposed in some studies (Demars 1978; Swanson and Jones 1982; Summers and Nyman 1985; Yuan et al. 2012). The pipeline failures that took place in the Gulf of Mexico during 1971–1975 were analyzed by Demars (1978). This analysis assumed the lateral pipe–soil interaction comparable to a cable carrying a suspended load—that is, the bending moment and shear forces generated in the pipe during the impact was ignored. It was shown that the pipelines experience the greatest magnitude of tensile force when the axis of a buried pipeline is parallel to the direction of debris flow and the least when perpendicular. This opinion was supported by Swanson and Jones (1982) while studying the effects of mudslide impact on pipelines in the Mississippi Delta. They developed a mathematical model to quantify the drag force on the pipelines. The over simplifications from Demars (1978) lead them to an erroneous and opposite conclusion that pipelines experience greater drag force when slide occurs in a direction parallel to the pipeline axis than slides occurring in perpendicular direction. The geometrical nonlinearities (large lateral displacement) of pipelines, nonlinear longitudinal soil resistance and nonlinear material property of pipeline (up to a limited extent) were considered in the studys done by

Summers and Nyman (1985). This analysis was based on the principle of virtual work. This simplified analytical approach could successfully quantify the maximum drag force, bending stresses and tensile force correctly.

Numerical modelling technique has also been adopted by a number of researchers. For example, Zhu and Randolph (2009) conducted a large deformation finite element (LDFE) modelling using a 'remeshing and interpolation technique with small strain' (RITSS) method and investigated debris flow impact on surface laid and buried pipelines. In this analysis, the pipe was initially placed within the debris mass (inconsistent with practical scenario) for the sake of numerical analysis and the debris block was forced to slide in downslope direction. The shear strength of seabed was identified as a key parameter that can affect the drag force and process of engulfment of the partially embedded pipelines. A numerical model using computational fluid dynamics (CFD) approach was developed by Zakeri et al. (2009). The laboratory flume-test results done by Zakeri et al. (2008) were simulated in this study. The dynamic viscosity of the debris (slurry) was modelled using Power-law rheological model. They successfully developed a practical method to quantify the drag force on surface-laid and suspended pipelines. The test data of Zakeri et al. (2008) were reanalyzed by Randolph and White (2012) and a combined approach (combination of geotechnical and fluid mechanics approach) to estimate the drag force on offshore pipelines was proposed. Zakeri and Hawlader (2013) developed another computational fluid dynamics (CFD) model based on the centrifuge tests conducted by Chi (2012). In this analysis, the clay block impacting the suspended pipe was modelled as a non-Newtonian fluid using the Herschel-Bulkley model. A simple approach of estimating the drag force on suspended pipes caused by a glide block impact was proposed combining the CFD results with the centrifuge test results. The ultimate bearing capacity of a 'wished in place' pipe was studied by Martin and White (2012) adopting the

limit equilibrium approach using OxLim (a FE limit analysis software developed at Oxford University). This analysis provided with a guideline to determine the undrained capacity of a pipe section considering a wide range of pipe-soil interface conditions, soil types and depths of embedment. Unlike Zakeri and Hawlader (2013), in this study, the model pipe was dragged laterally and vertically to determine the lateral, penetration and uplift resistances. Dutta and Hawlader (2018) also adopted CFD approach to simulate lateral penetration of a suspended pipe in a clay block. The strain-rate and strain-softening effects on clay were incorporated in the analysis. Saha et al. (2018) modelled large deformation problems using CFD and Coupled Eulerian-Lagrangian (CEL) approaches and concluded that CFD approach is computationally efficient. However, there was no clear indication of the effect of seabed strength and gap between the pipeline and seabed on the drag force on suspended pipelines caused by the debris impact.

Physical modelling through small scale testing and centrifuge testing have been conducted by a number of researchers (Brookes and Whitmore, 1968; Paulin et al. 1995, 1998; Phillips et al. 2004; Oliveira et al. 2009; Zakeri et al. 2008; Chi, 2012; Sahdi et al. 2014). Among all these studies, Zakeri et al., (2008) and Chi (2012) were focused on the suspended pipelines only. Zakeri (2008) performed a series of laboratory flume tests with Kaoline clay slurry to study the impact of clay-rich debris on suspended pipes. On the other hand, Chi (2012) set up a centrifuge modelling technique to model the impact of a sliding glide block on a suspended pipeline placed at a position halfway from the top of the glide block. Later, Drago et al. (2015) investigated the effect of seabed strength and seabed roughness on current and wave action on the free-span pipelines and showed that the hydrodynamic loading on the suspended pipelines can significantly be affected by seabed parameters. Moreover, Slingsby (2015) demonstrated that the gap under the suspended pipeline might play an important role in modelling the Vortex Induced Vibration (VIV) impact on the free-

span pipelines. The insights of these two researches led this study to investigate the effects of seabed soil strength and gap beneath the pipe on the drag force generated during a landslide impact on the suspended pipelines.

## 4.3 Problem statement

After the initiation of a submarine landslide, a failed soil mass moves along the downslope with a velocity $v_0$ and impacts a suspended pipeline of diameter $D$ located at a normalized depth of $\hat{w}$ (=$w$/$D$, where $w$ is the depth of the bottom of the pipe from the top surface of the debris) and at a normalized height $\hat{g}$ (= g/$D$) above the seabed surface (Fig. 4.1). Generally, submarine slopes are mild; therefore, in the present numerical analysis, the seabed is assumed to be horizontal. For the same reason, the vertical component of the velocity of the debris is ignored and the failed soil mass is considered to move laterally only in the horizontal direction. The front face of the sliding soil mass might have an irregular shape due to the complex soil–water interaction during downslope movement; however, for simplicity, the front face is assumed to be inclined at an angle $\theta = 45°$ to the horizontal. As the impact velocity is very high, an undrained behaviour of soil (both debris and seabed soil) govern the response. This study is limited to a single burial depth ($\hat{w} = 3$); however, the gap between the pipe and seabed has been varied from $\hat{g} = 0.5$ to 3.0 by varying the depth of seabed.

## 4.4 Numerical modelling

### 4.4.1 Basic concepts of CFD modelling

General purpose ANSYS CFX 16.2 software package has been used for numerical modelling (ANSYS CFX, 2015). The solution technique of CFX is based on a finite volume technique, so the entire domain has been discretized into many small control volumes through three-dimensional

meshing. These small control volumes are also termed as elements. The conservation of general dependent variables, φ of materials flowing through the control volume is the basic principle of CFX formulation. The transport equation can be expressed in a generalized form as:

$$\frac{\partial}{\partial t}(\rho\varphi) + \text{div}\,(\rho\varphi\mathbf{u}) = \text{div}(\Gamma \text{grad}\varphi) + S_{\varphi} \quad (4.1)$$

Here, ρ represents the density of material flowing through the control volume; **u** denotes the velocity vector; Γ is the diffusion coefficient and $S_{\varphi}$ is source terms used for modeling actual physical rates of internal generation. The first term in Eq. (4.1) represents the rate of change of variable of the material flowing through the control volume; the second term denotes the change due to advection; and the third term stands for the variation of φ from one point to another point within the domain.

In ANSYS CFX, the process of mass and momentum transfer has been modelled by the Navier–Stokes equations, which is based on Newton's second law of motion of fluids (i.e. soft clay and water in this study). In pipe–soil–water interaction problems, the force acting on an element comprises of two parts: (i) surface force due to the pressure and viscous force and (ii) gravitational force. The pressure is analogous to the normal stress in solid mechanics which represents the normal stress acting on the surface of an element (control volume) and the viscous force is a result of shear stress of the flowing fluid. The pressure and viscous forces (i.e. surface forces) on an element are incorporated by the third term of the momentum equation, whereas, the gravity force (i.e. body force) is incorporated by the forth term of Eq. (4.1). The modelling of the viscous forces in clay is a critical step while modelling pipe–soil–water interaction. In this study, this is performed using the coefficient of dynamic viscosity of clay as a function of the undrained shear strength of clay.

$$\mu_d = \frac{s_u}{\dot{\gamma}} \tag{4.2}$$

Where, $\mu_d$ is the dynamic viscosity of clay, $s_u$ is the undrained shear strength and $\dot{\gamma}$ is the clay shear strain rate.

### 4.4.2 CFD Model development

#### *4.4.2.1 Geometry and boundary conditions*

General purpose ANSYS CFX 16.2 software package is used for numerical modelling (ANSYS CFX, 2015). Typical geometry and boundary conditions used in numerical models (for $w = 3D$ and gap, $g = 3D$) are shown in Fig. 4.2. Since CFX allows three-dimensional modelling only, all the analyses are performed for one element of 10-mm thickness in the out-of-plane direction. A 290-mm diameter and 10-mm long stationary rigid pipe is placed at a depth of 885 mm from the top of the clay block and the gap between the pipe and seabed is varied by varying the depth of seabed (e.g. a 290-mm deep seabed is used for $g = 3D$; a 580-mm deep seabed for $g = 2D$). The domain is discretized using a three-dimensional mesh, where 'face mesh sizing' technique in CFX is used to generate finer mesh in a zone around the pipe. Mesh deformation is not allowed in this analysis; hence the shape and size of elements remain unchanged with loading. Both the soil and water are modelled as Eulerian materials that flow through the fixed mesh and thus the numerical issues related to mesh distortions are avoided.

All the boundaries are placed sufficiently far from the pipe to avoid the boundary effects. The left boundary is defined as an inlet by defining differential inlet velocities—the lower part (up to the depth of seabed) is kept stationary with $v_x = v_y = v_z = 0$ and the upper part (above the seabed) is modelled to allow the flow of materials as an inlet with $v_x = v_0$. This allows soil and water to get in to the domain at a constant velocity, $v_0$ over the seabed. Similar differential velocity boundary

condition is also used at the right boundary to allow soil and water exiting the domain. The right boundary is placed sufficiently far away from the pipe that enables the formation of a channel behind the pipe after the impact, as discussed later. The bottom boundary is modelled as an impermeable wall to restrict the flow of water and soil through the bottom boundary. A thin layer of weak material is used between the seabed and sliding soil mass to allow the soil mass sliding freely. A plane symmetry boundary condition is used at the vertical faces of the domain. The top surface of the domain is defined as opening to allow water to flow in and out of the domain.

The water–soil interface (abcd) is defined using the volume fraction tool, volume fraction for clay is taken as 1 and 0 for water within the block abcdef. While, for rest of the domain (abcdhg), it is reverse.

The pipe is designed as an impermeable wall with no-slip condition. The concept of finite thickness interface element (Supachawarote et al., 2004; Jostad and Andresen, 2004) is used to model the pipe–soil interface. The undrained shear strength of a finite thickness element (7.25 mm) is modelled as $\alpha s_u$, where $\alpha = 1$ represents rough condition and $\alpha = 0$ represents smooth interface condition. A constant value of $\alpha = 0.5$ is used for modelling the soft clay–pipe interaction. In this study, $s_u$ implies undrained shear strength of clay in plane strain condition, unless otherwise mentioned.

#### *4.4.2.2 Undrained shear strength of clay*

Experimental evidence suggests that the undrained shear strength of clay ($s_u$) depends upon shear strain rate ($\dot{\gamma}$) and magnitude of accumulated plastic shear strain ($\xi$). For clays, $s_u$ increases with $\dot{\gamma}$ and decreases with $\xi$. In order to capture the effects from these two factors, Einav and Randolph (2005) proposed the following equation.

$$s_u = f_1 f_2 s_{u0} \tag{4.3}$$

where, $f_1$ and $f_2$ represent the effects of strain rate and strain-softening respectively; $s_{u0}$ is the reference (initial) undrained shear strength at a reference shear strain rate ($\dot{\gamma}_{ref}$) prior to any softening. In the present study, $f_1$ and $f_2$ are calculated using the following equations (Einav and Randolph 2005).

$$f_1 = 1 + \mu \log\left\{\frac{max\left(\dot{\gamma}, \dot{\gamma}_{ref}\right)}{\dot{\gamma}_{ref}}\right\} \tag{4.4}$$

$$f_2 = \frac{1}{S_t} + \left(1 - \frac{1}{S_t}\right) e^{-3\xi / \xi_{95}} \tag{4.5}$$

Where $\mu$ is the rate of change of $s_u$ per log cycle of strain rate; $S_t$ is the remoulded sensitivity; and $\xi_{95}$ is the value of $\xi$ at 95% reduction of shear strength of soil due to remoulding.

## 4.5 Parameter selection

The geometry and soil properties used in the 'base case' analysis is listed in Table 4.1. Both soil and water are modelled as homogenous multiphase Eulerian material by defining the shear behaviour in terms of dynamic viscosity. For water, a constant dynamic viscosity is used. The clays in debris and seabed are modelled as visco-plastic non-Newtonian fluids. In deep water, a linear increase of undrained shear strength with depth—a crust in some cases—has been observed. However, in the present study, a uniform undrained shear strength of debris ($s_{u0,d}$) of 5 kPa and seabed ($s_{u0,b}$) of 10 kPa are used for the base case analysis. In the parametric study, the analyses have been performed for varying $s_{u0}$.

## 4.6 Base case analysis results

*Force–displacement behaviour*

Figure 4.3 shows the variation of normalized horizontal drag force on pipe, $N_h$ (= $F_x/s_{uN}D_eL$) with normalized horizontal penetration distance, $\hat{u}$(= $u/D_e$). Here, $F_x$ is the horizontal component of the drag force on the pipe; $s_{uN}$ is the value of $s_u$ used for normalization ($s_{uN} = 2/\sqrt{3}$ ($s_{u0,d}$), Hawlader et al. 2015); $D_e$ is the effective diameter; $L$ is the length of the pipe in the out of plane direction; and $u$ is the lateral penetration distance of the pipe into the debris. A fully-bonded no-slip interface condition is used for modeling the soil–pipe and soil–water interface behaviour. Therefore, it is assumed that shear failure occurs at the mid-thickness of the elements immediately outside the outer surface of the pipe. These elements can be considered as 'finite thickness interface elements.' Following the assumption of Gui and Bolton (1998), the effective diameter of the pipe ($D_e$) is calculated as 295 mm (= 290 mm + 2 × 5/2 mm), where the thickness of the 'finite thickness interface elements' is ~ 5 mm for the CFX model used in the present study. The lateral penetration distance ($u$) at any instant ($t$) is calculated as $u = v_0(t\text{-}t_0)$; where, $v_0$ is the velocity of the sliding soil mass; $t_0$ is the time when the soil mass touches the pipe and the drag force on the pipe starts to increase.

Figure 4.3 shows the force–displacement curves for a burial depth of 3$D$ and five gaps ($g$ = 0.5$D$–3.0$D$). For this given burial depth (3$D$), the horizontal force on the pipe increases with an increase in gap. No significant difference between the force–displacement curve is found for $g \geq 2.0D$. The potential mechanisms behind this are described in later sections. For $g \geq 2.0D$, the normalized lateral force ($N_h$) increases quickly with normalized lateral penetration distance ($\hat{u}$) until $\hat{u}$ ~ 2–3. After that, $N_h$ continues to increase but at a slower rate than that at $\hat{u} \leq 2$. The $N_h$ remains constant (~ 11.8) at $\hat{u} \geq 12$.

The initial segment of the force–displacement curve (i.e. for $\hat{u} \leq 2$) for smaller gaps ($g \leq 1.5D$) is similar to those of $g \geq 2.0D$, although the normalized lateral force increases with the gap. For $g \leq 1.5D$, the normalized force decreases with penetration distance after $\hat{u} \sim 2$ and becomes almost constant after at $\hat{u} \sim 12$.

These analyses confirm that the gap plays a significant role on the drag force. For the cases analyzed in this study, the maximum drag force ($N_h \sim 11.8$) on the pipe is found for a large gap ($g \geq 2.0D$), which is almost the double of the $N_h$ (~ 6) for small gaps of $g = 0.5D$–$1.0D$ at a large penetration distance and 50% higher than the peak $N_h$ (~ 8) for the same small gaps.

Another important aspect related to numerical issues also needs to be considered in this type of large deformation analyses. The pipe needs to be penetrated a significantly large distance (e.g. ~ 12$D$ for a large gap in Fig. 4.3) to reach the maximum lateral force. A conventional finite element method (FEM) in the Lagrangian framework cannot simulate such a large deformation because of significant mesh distortion issues. An advanced FEM, such as the Coupled Eulerian–Lagrangian (CEL) approach, can be used to avoid numerical issues related to mesh distortion. However, Dutta and Hawlader (2018) showed that CEL modelling is computationally very expensive as compared to the CFX approach presented here. Therefore, a CFD approach, as the one presented in this study, might be a better choice for modelling the drag force.

*Soil particle velocity and role of free water*

Figure 4.4 (a) shows the instantaneous velocity of clay particles at a large penetration distance of $u = 12D$ in the simulation of 3$D$ gap between the pipe and seabed. The change in instantaneous velocity, both magnitude and direction, primarily occurs around the pipe and interfaces (e.g. at pipeline–soil interface and bottom boundary). A cavity is formed behind the pipe when the soil

flows around it. The cavity is filled with 'free water.' Note that the role of this free water is different from pore water in the soil.

The accumulation of plastic shear strain ($\xi$) is also shown in Fig. 4.4(a). Note that $\xi$ cannot be obtained directly from the CFX analysis; therefore, the method developed by Dutta and Hawlader (2018), based on the incremental strain in each time increment, is used to calculate $\xi$. Figure 4.4 shows that, in this case, large plastic shear strain mainly generates along the seabed–debris and pipe–soil interfaces. A large plastic shear strain also generates in the soil elements near the interface between the sliding debris separated by the pipe (along line AB), which is due to the difference in instantaneous velocity in upper and lower soil elements. Note that plastic shear strain can also generate in the seabed soil, especially for a low seabed shear strength case, which also depends upon the gap ($g$), as discussed in a later section.

For a small penetration distance (e.g. $u \leq 2D$, Fig. 4.3), the channel behind the pipe—forms due to the flow of debris—remains open and connected to water outside the debris. However, at a large penetration distance (e.g. $u > 4D$, Fig. 4.3), the channel becomes narrow or closed at a distance sufficiently far from the pipe. At this stage, the water in the cavity behind the pipe becomes isolated from the water outside the clay block or connected by the constricted channel. The displacement of soil causes suction in the water in the cavity (negative of hydrostatic pressure).

Figure 4.4(b) shows the suction behind the pipe for $u = 12D$. The maximum suction of ~ 25 kPa develops immediately behind the pipe at this stage. The suction is zero when the channel behind the pipe is large, as the water in the channel can flow easily. The suction increases when the channel becomes narrow. The suction also accelerates the closing of the channel. At a very large penetration, only a small cavity remains behind the pipe.

The change in velocity due to the obstruction of the pipe causes surface heave. Note that the surface heave depends on the size of the gap and undrained shear strength of the soil, as discussed in the following sections.

On the contrary, lower gap beneath the pipe (< 2*D*) causes hindrance to pass through the bottom of the pipe and creates a retaining type structure behind the pipe (Figs. 4.6 (a)–4.8 (a)). Formation of similar type of rigid wedges behind the pipe during the landslide has been also mentioned by Zhang et al. (2016). This rigid wedge beneath the pipe prevents the formation of a closed channel behind the pipe which eventually causes reduction of free-water-suction on the pipe. Figures 4.4 (b)–4.8 (b) depict the variation of suction on the pipe due to the gap effect—in case of 2*D*–3*D* gaps, the suction around the pipe is 13–25 kPa; whereas, this value falls to 1 kPa (or even 0 suction) in case of 0.5D gap. This reduced suction causes a lower drag force on the pipeline. So, from the design point of view, as the greater is the gap beneath the pipe, the higher will be the drag force (for same burial depth). The gap effect remains the same for gaps higher than 3*D*, so analyses are done up to $g = 3D$.

## 4.7 Parametric study

A wide range of undrained shear strength of clay sediments in deep sea environments has been reported in the literature (Boukpeti et al. 2009). In addition, the shear strength of the failed clay block, which is originated from the seabed of varying shear strength, decreases with downslope movement, primarily due to strain-softening and interaction with surrounding water and seabed (Boukpeti et al. 2012). In this section, a parametric study is performed by varying the shear strength of debris and/or seabed, while keeping the other parameters the same as the base case.

### 4.7.1 Strength of seabed sediments

Figure 4.9 shows the variation of the maximum normalized horizontal drag force, $N_{h(max)}$ (= $F_{x(max)}/s_{uN}D_eL$) for a given initial shear strength of the debris ($s_{u0,d}$ = 5 kPa) but for varying gap ratios ($\hat{g}$ = 0.5–3) and initial shear strength of the seabed ($s_{u0,b}$ = 2–10 kPa). The maximum drag force is obtained by plotting the normalized force with normalized penetration, as shown by the circles in Fig. 4.3. The following are the key observation, for the cases analyzed.

i) The maximum normalized horizontal drag force ($N_{h(max)}$) increases with the normalized gap ($\hat{g}$) up to ~2.0. After that, the $N_{h(max)}$ remains almost constant for a given base shear strength.

ii) For a small gap ($\hat{g}$ = 0.5), no significant difference between the maximum normalized force is obtained. However, a considerable difference is found for different seabed strength at larger gaps.

iii) Generally, $N_{h(max)}$ is smaller for large seabed shear strength (e.g. $s_{u0,b}$ = 10 kPa) than that of small seabed shear strength (e.g. $s_{u0,b}$ = 2 kPa). However, an opposite trend is found for larger gaps ($\hat{g} \geq 2$). Whenever the seabed is weaker than the debris and the gap is small ($g < 2D$), the stronger debris material pushes the seabed material beneath the pipe and makes a way out to go through the narrow gap. This enables the formation of a closed channel behind the pipe and free-water suction develops behind the pipe that causes a higher $N_{h(max)}$. Even in case of higher gaps under the pipe, whenever there lies softer seabed (i.e. $s_{u0,b} < s_{u0,d}$) underneath the debris mass, the stronger debris mass pushes the weaker seabed materials (Fig. 4.10) and as a result, berm height over the pipe decreases which causes reduction of $N_{h(max)}$ in case of weaker seabed in higher gap ($g \geq 2D$) conditions.

### 4.7.2 Strength of debris materials

A total of 15 analyses are performed for a varying debris strength (1 kPa–5 kPa), while keeping the other parameters same as the base case. Note that, in these simulations, the seabed is stronger than the debris ($s_{u0,b}$ = 10 kPa). Figure 4.11 shows that, at a small gap ($\hat{g} \leq 2.0$), the maximum normalized force ($N_{h(max)}$) is significantly smaller for a larger debris strength (e.g. $s_{u0,d}$ = 5 kPa) than a smaller one (e.g. $s_{u0,d}$ = 5 kPa). However, the difference is small at larger gaps ($N_{h(max)}$ = 11.7–12.6).

For a large $s_{u0,d}$, the debris cannot flow thorough a small gap between the pipe and seabed, as shown in Fig. 4.12 (b). However, if the debris strength is low, it can flow through the same small gap, resulting in easier closing of the channel behind it and increase in suction (Fig. 4.12 (a)). Therefore, a higher $N_{h(max)}$ is calculated for a low-strength debris. When the gap is large ($\hat{g} \geq 2.0$), the debris can flow through the gap, even for a large-strength debris considered in this study ($s_{u0,d}$ = 5 kPa); therefore, the difference in calculated $N_{h(max)}$ for varying debris strength is small.

## 4.8 Conclusions

This chapter concludes that the drag force on the suspended pipelines is strongly dependent on the suction developed behind the pipe. The gap ratio and shear strengths of seabed and debris altogether control the formation of the closed channel where suction force develops. A small gap ($g < 2D$) with stronger seabed does not allow the debris material to flow below the pipeline and prevents the formation of a closed channel behind the pipe. As a result, the drag force is significantly lower than the cases where there exists a large gap ($g \geq 2D$) under the pipeline. However, the scenario is altered when there exists weaker seabed below the pipeline. So, the bottom line of this research is that the maximum normalized drag force on suspended pipelines is controlled by the combination of gap ratio, seabed shear strength, and debris shear strength.

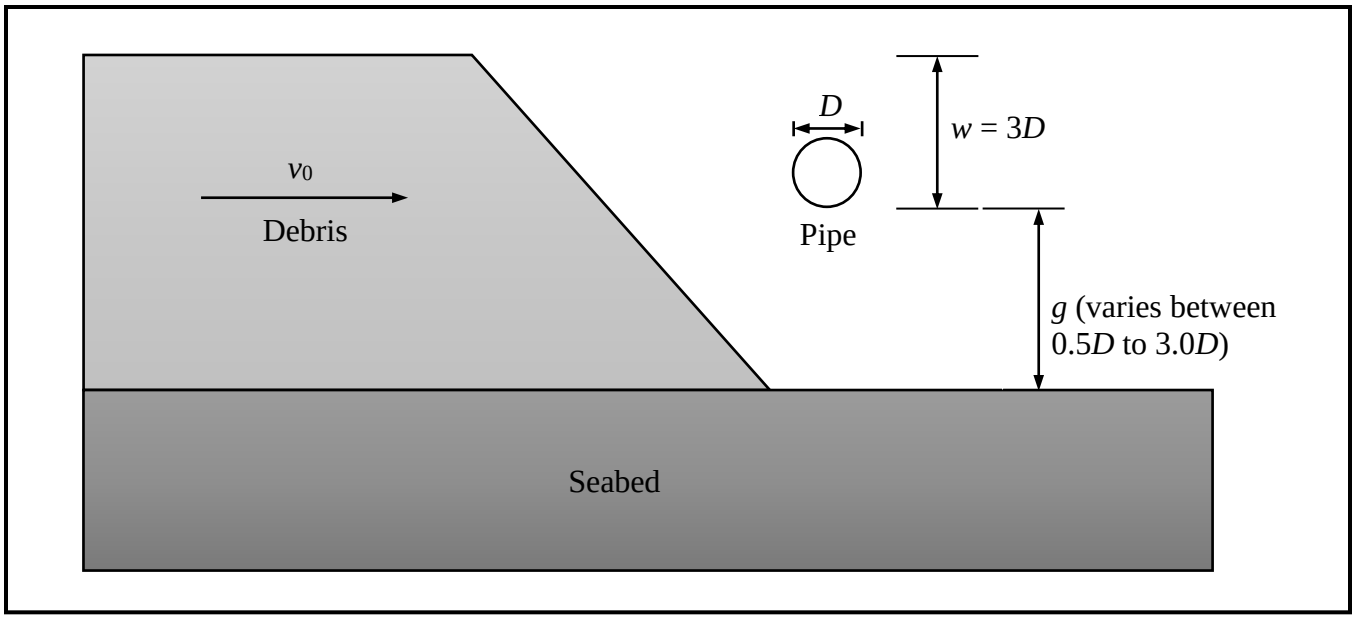


**Figure 4.1.** Problem definition

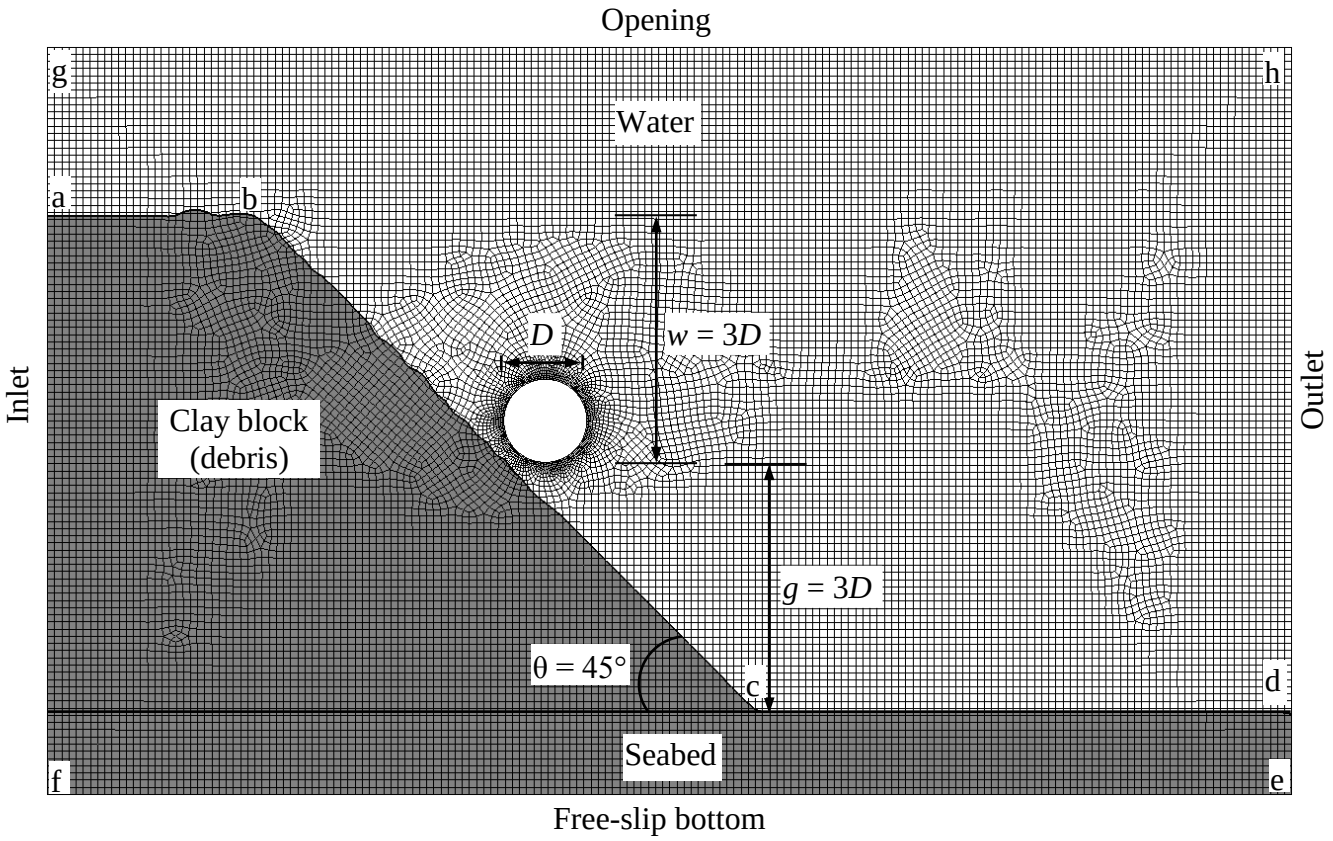


**Figure 4.2.** Typical finite volume modelling in ANSYS CFX, gap ($g$) = 3$D$

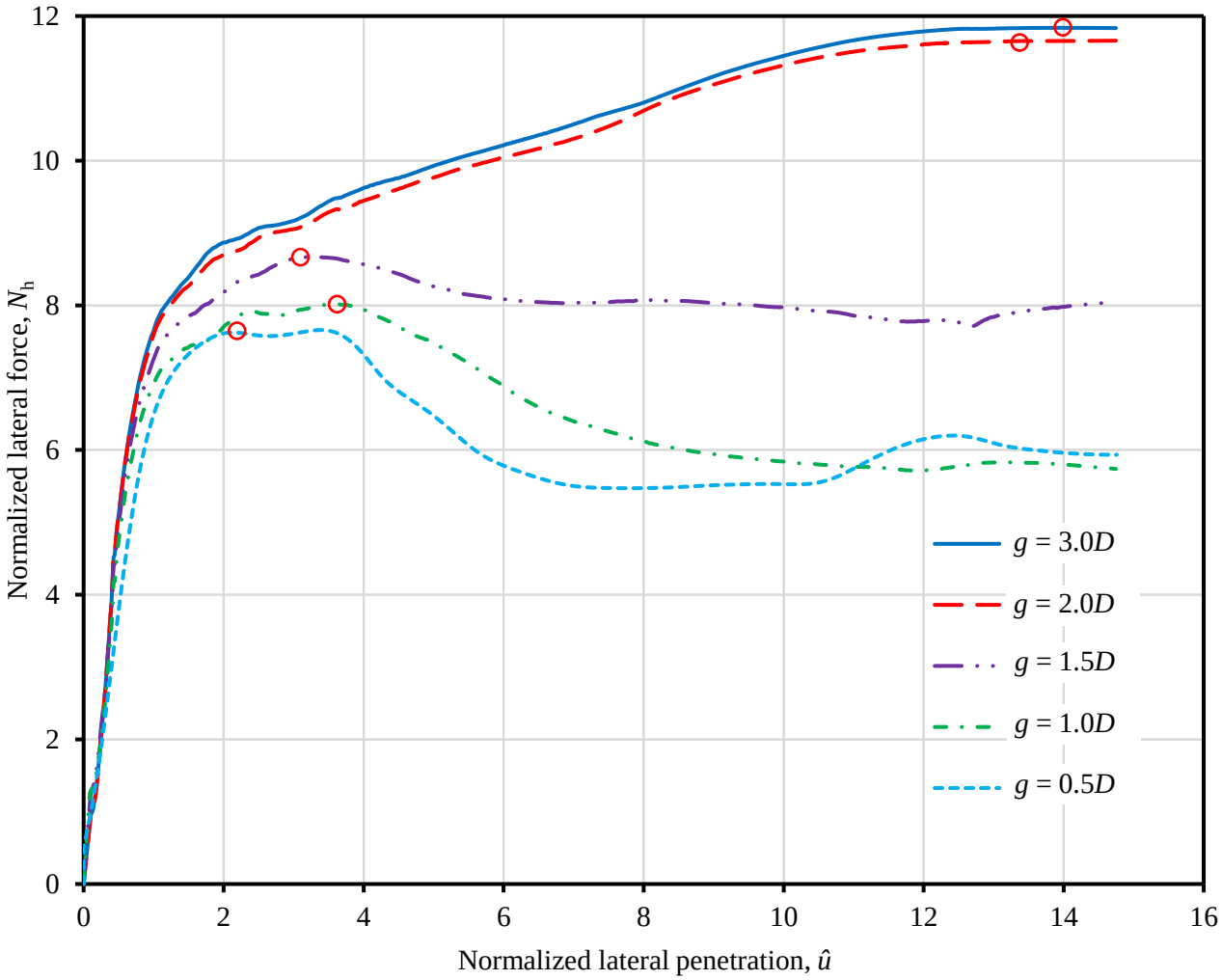


**Figure 4.3.** Normalized force–displacement curves for $s_{u0,d}$ = 5 kPa and $s_{u0,b}$ = 10 kPa

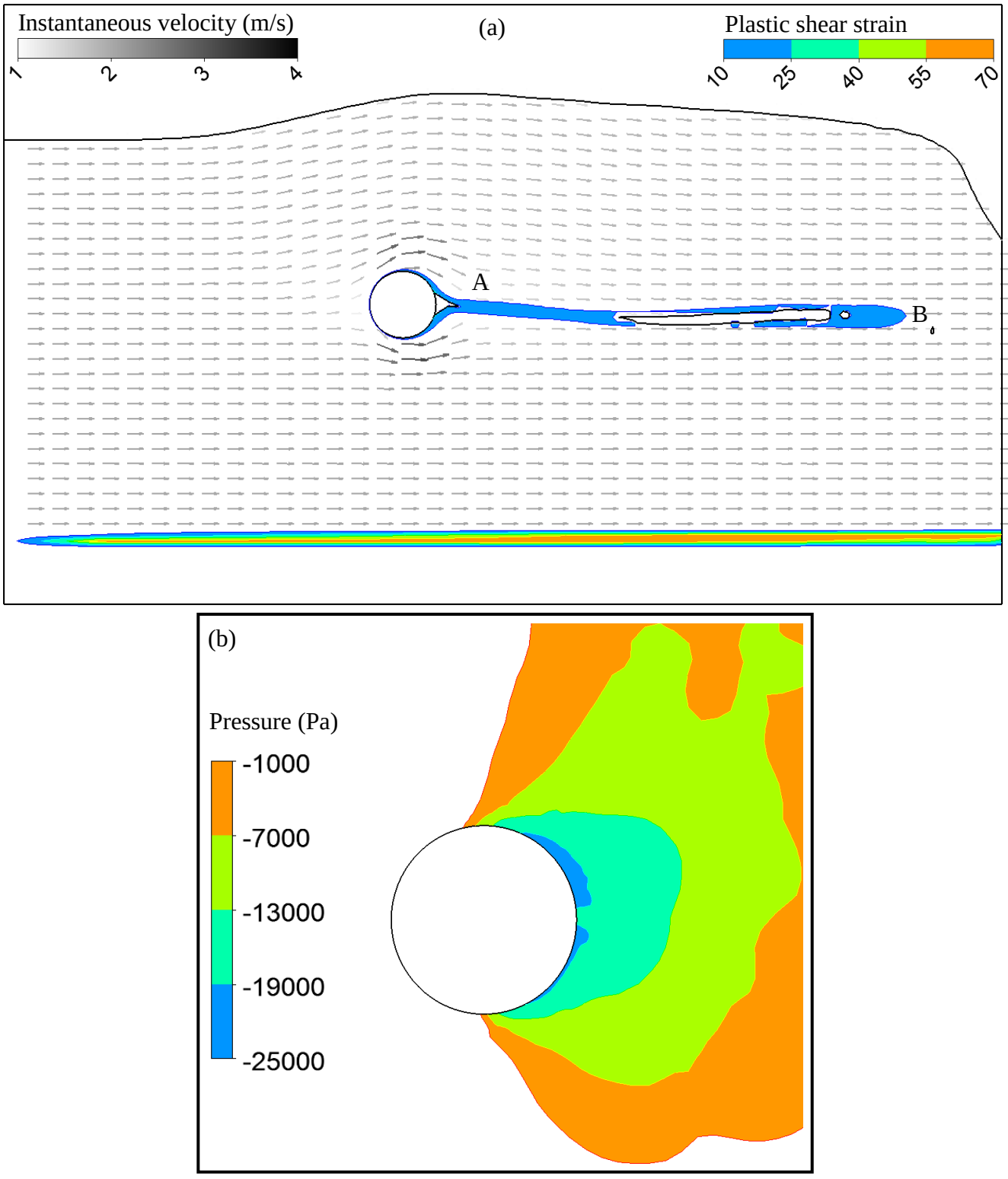


**Figure 4.4.** Typical response for 3D gap at $u = 12D$: (a) instantaneous velocity and plastic shear strain; (b) suction behind the pipe

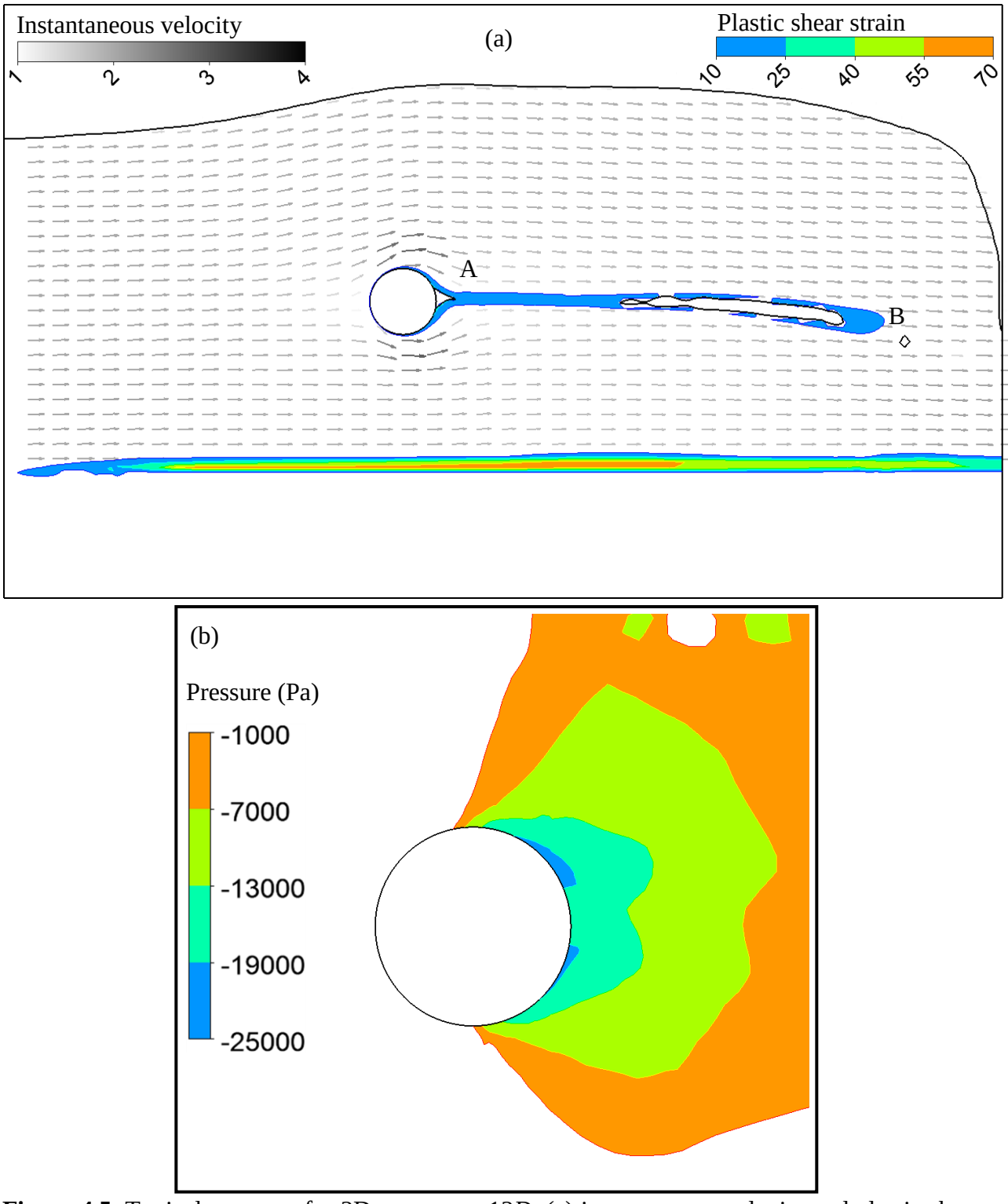


**Figure 4.5.** Typical response for 2D gap at $u = 12D$: (a) instantaneous velocity and plastic shear strain; (b) suction behind the pipe

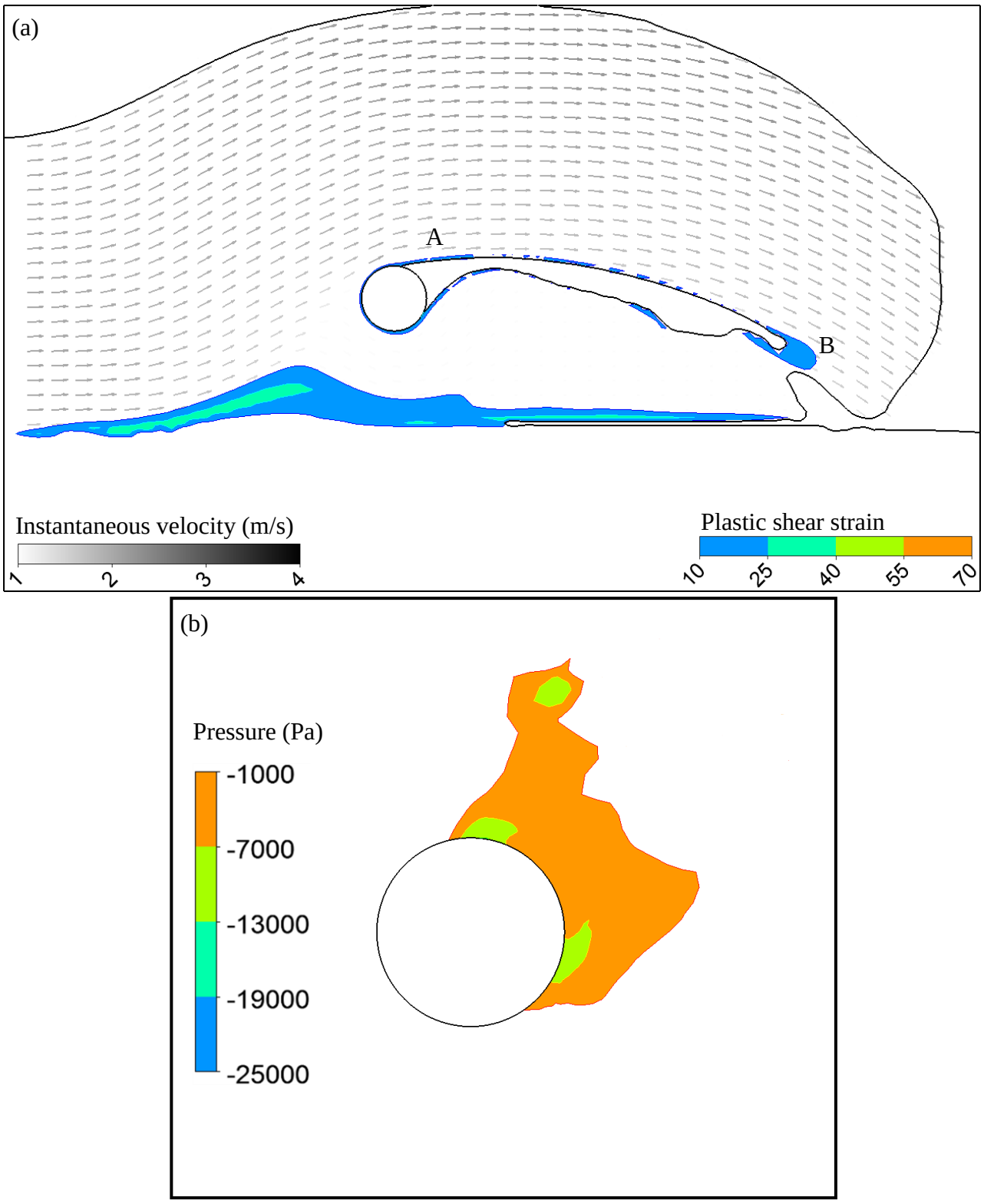


**Figure 4.6.** Typical response for 1.5*D* gap at *u* = 12*D*: (a) instantaneous velocity and plastic shear strain; (b) suction behind the pipe

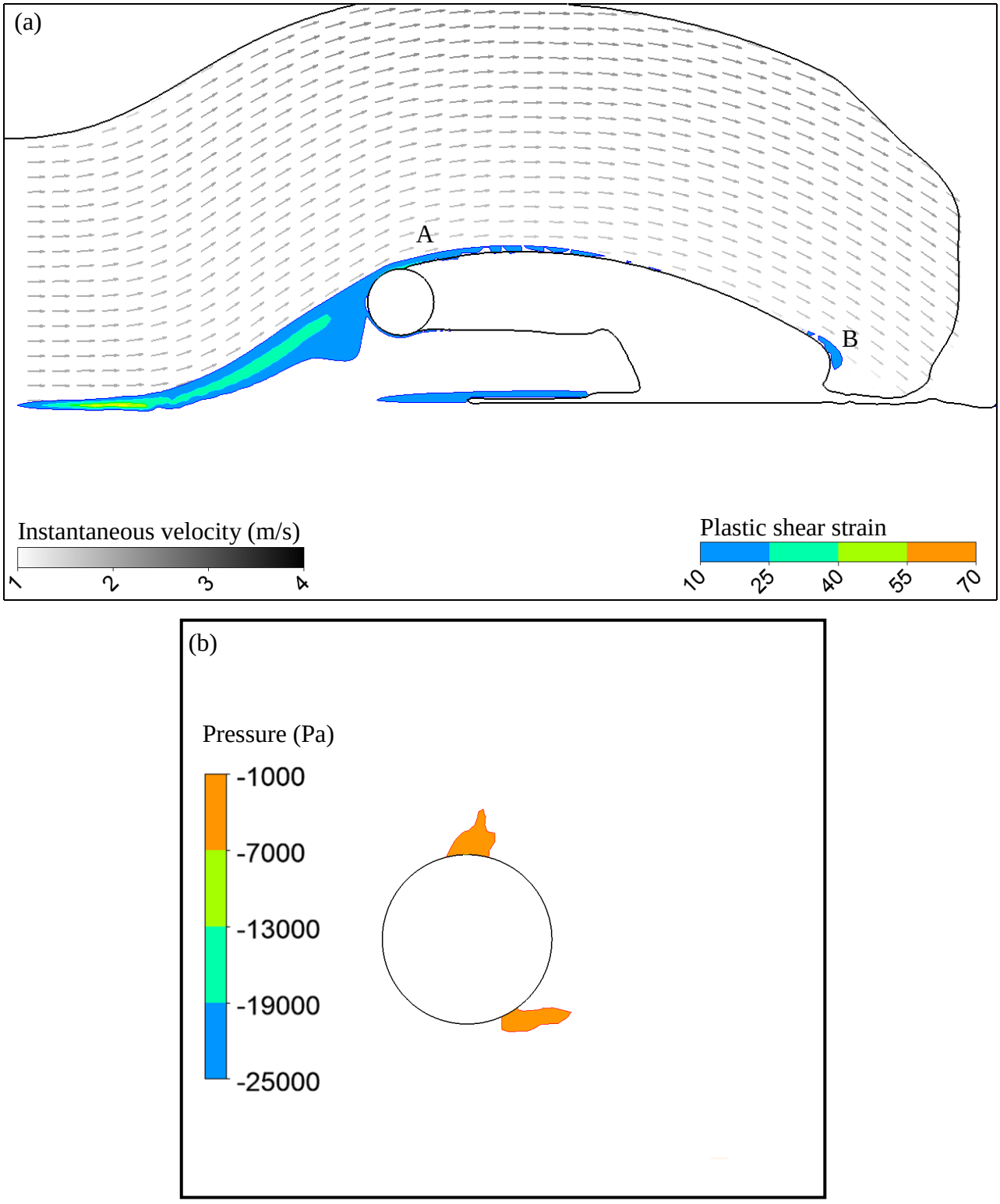


**Figure 4.7.** Typical response for 1*D* gap at *u* = 12*D*: (a) instantaneous velocity and plastic shear strain; (b) suction behind the pipe

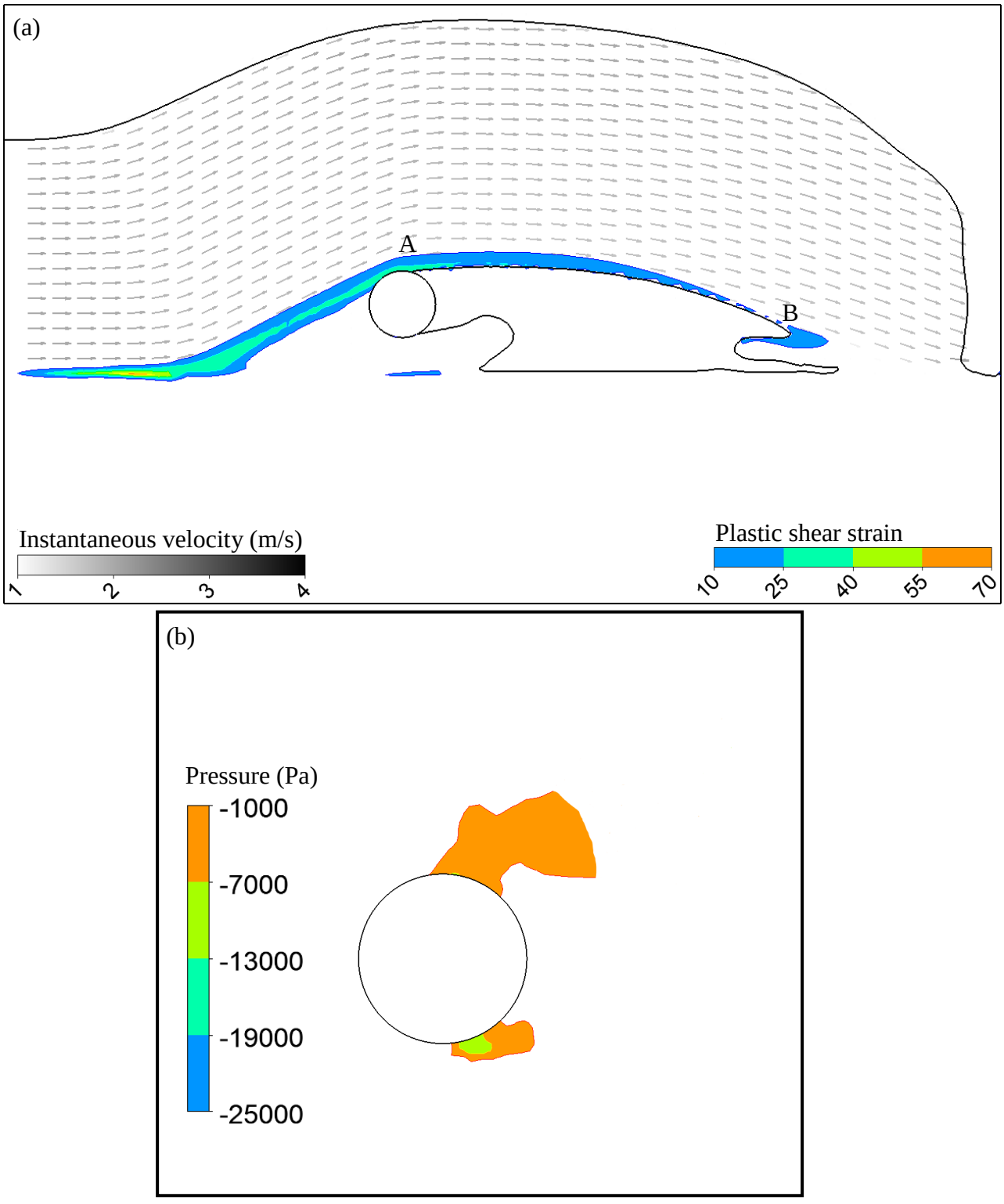


**Figure 4.8.** Typical response for 0.5*D* gap at *u* = 12*D*: (a) instantaneous velocity and plastic shear strain; (b) suction behind the pipe

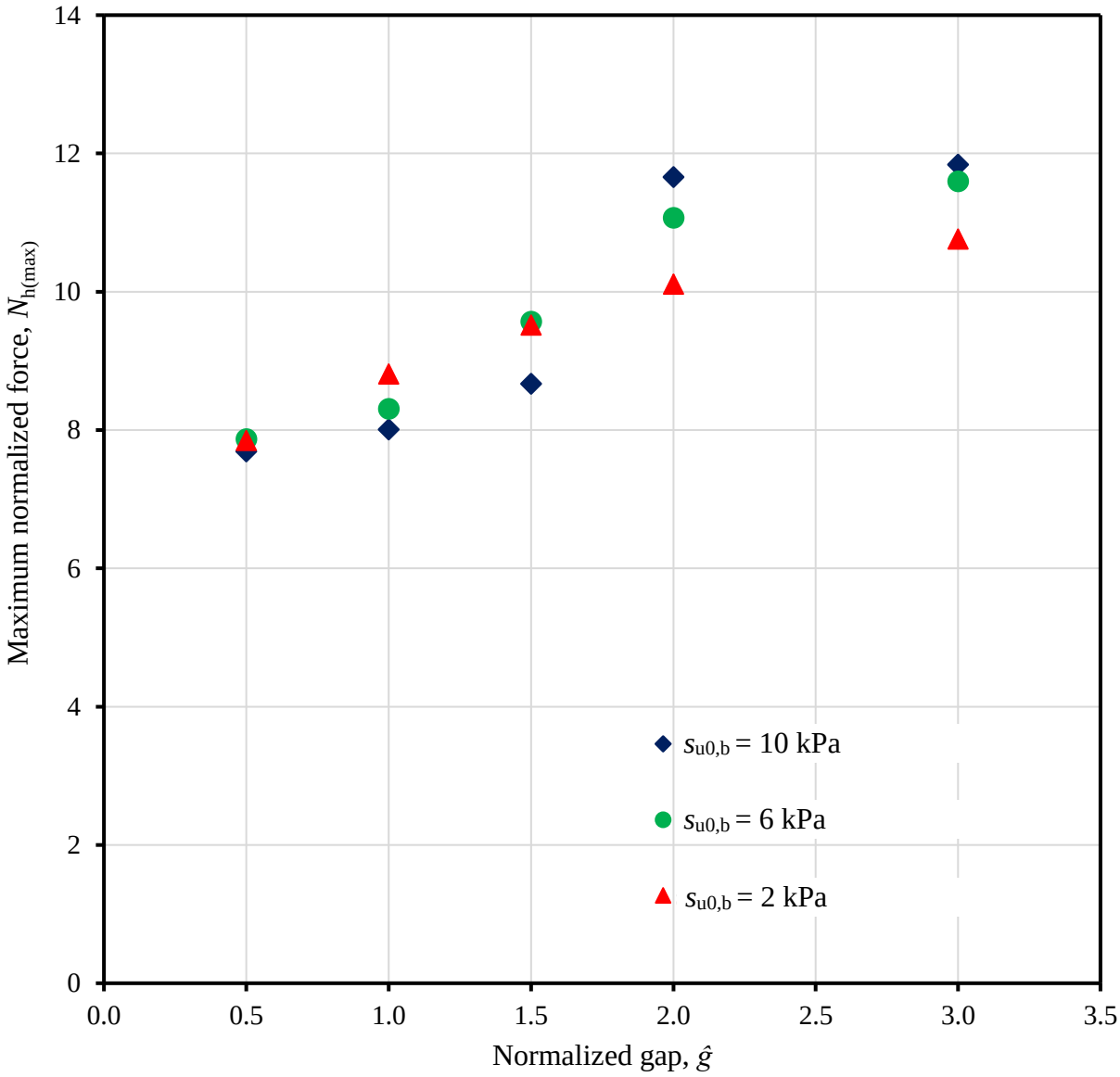


**Figure 4.9.** Maximum normalized horizontal drag force for varying seabed strength and gap ($s_{u0,d}$ = 5 kPa)

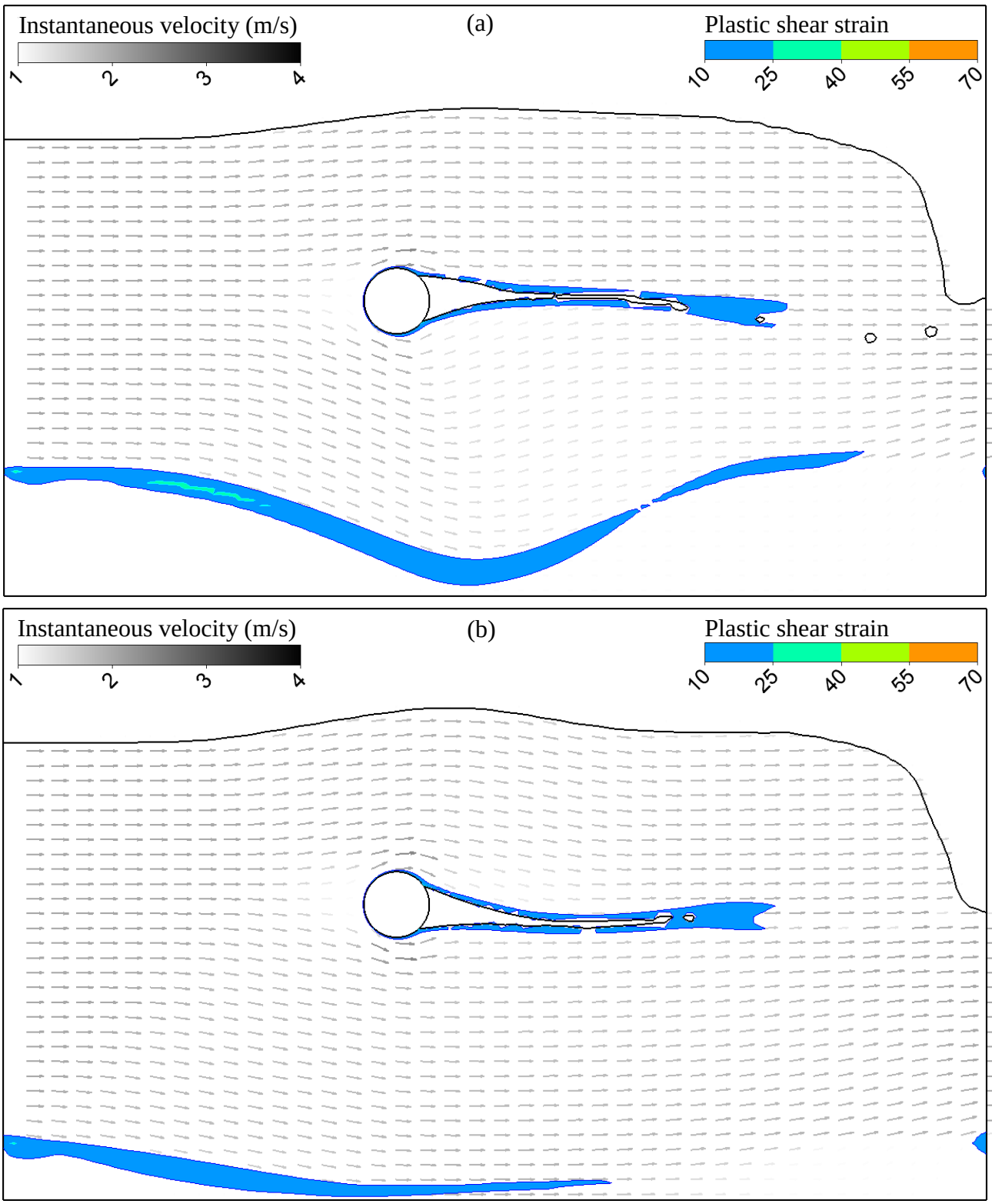


**Figure 4.10.** Typical strong debris–weak seabed interaction at: (a) $g = 2D$; (b) $g = 3D$

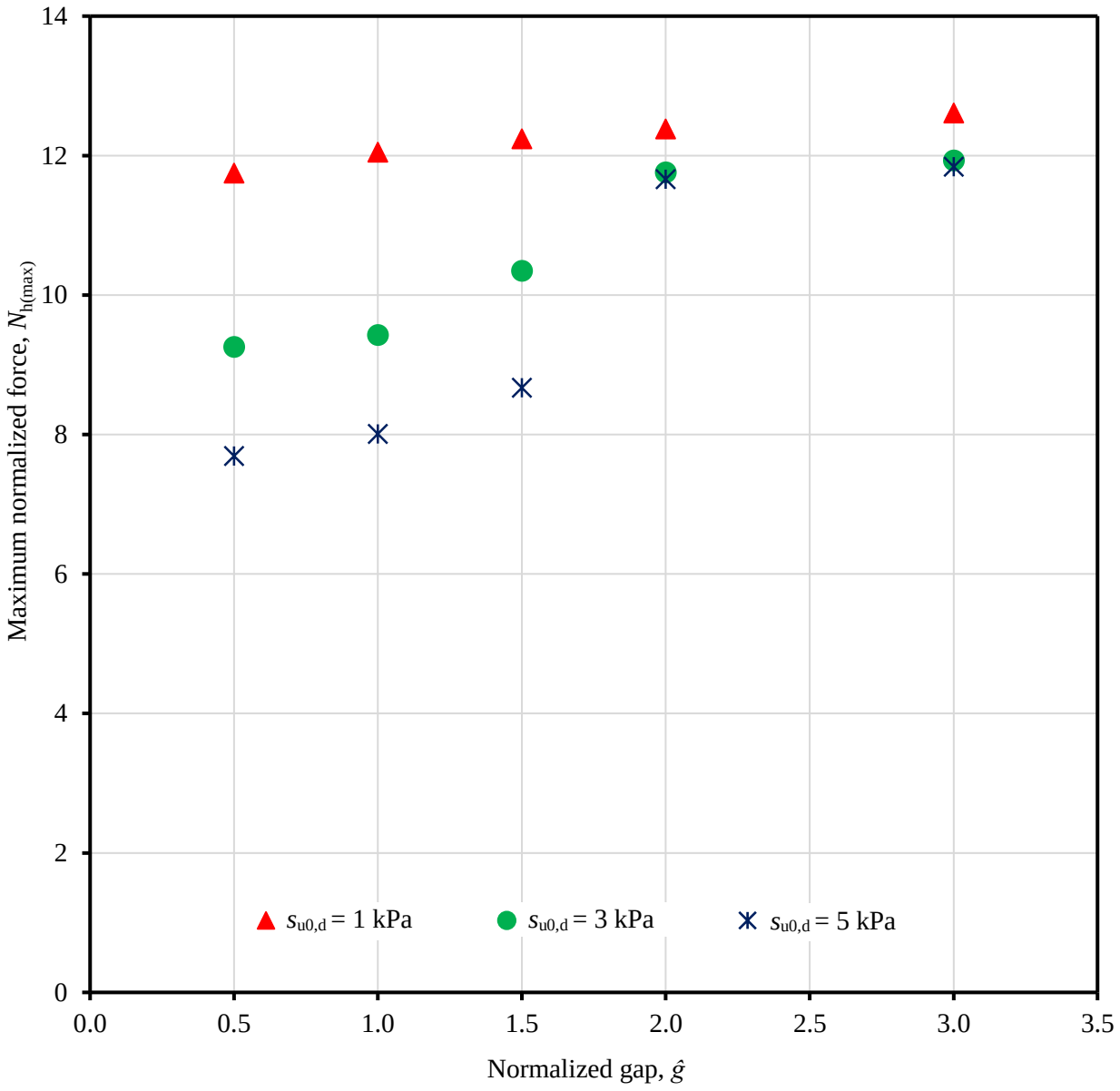


**Figure 4.11.** Maximum normalized horizontal drag force for varying debris strength and gap ($s_{u0,b}$ = 10 kPa)

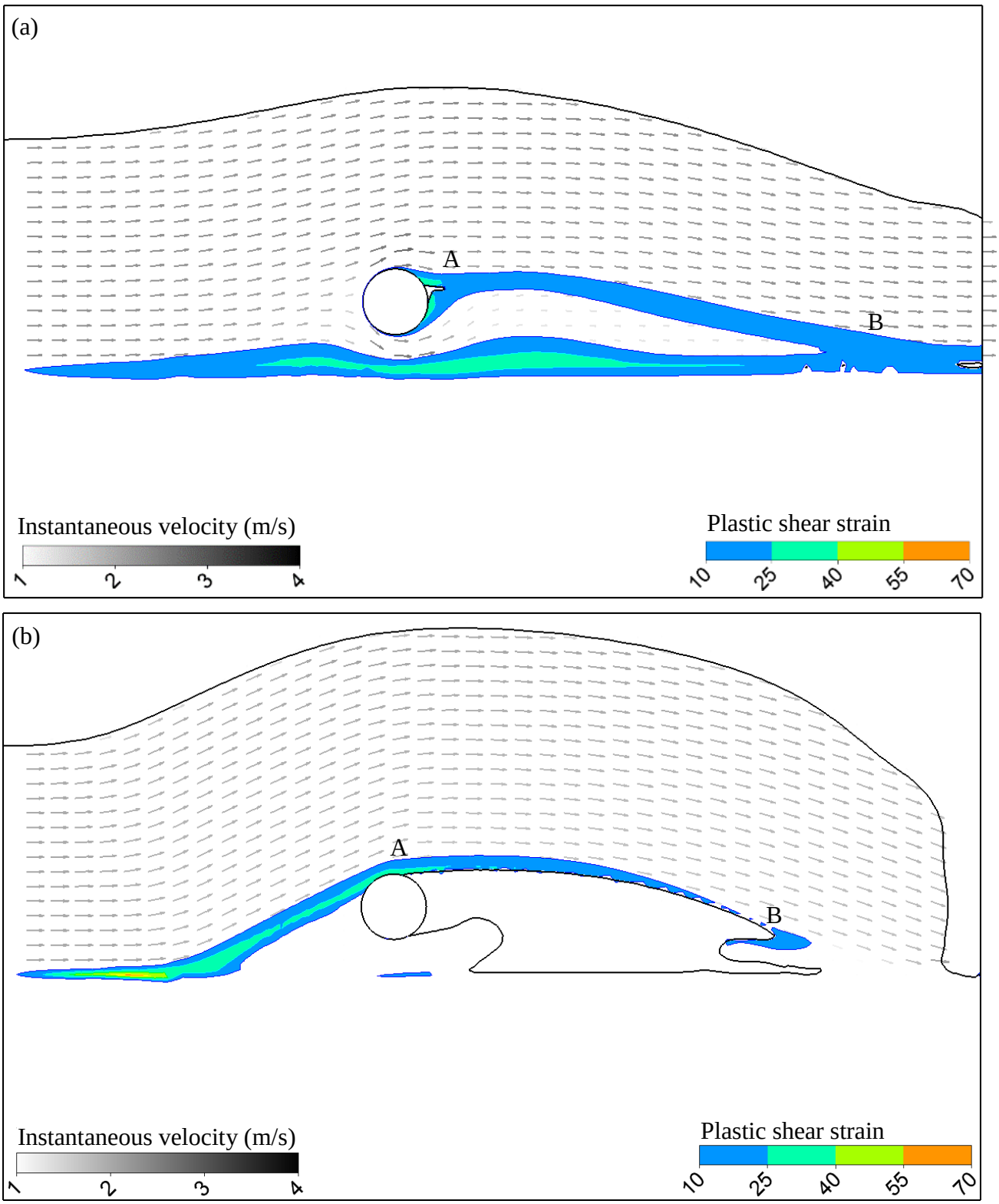


**Figure 4.12.** Debris flow mechanism through narrow gap ($g$ = 0.5$D$): (a) $s_{u0,d}$ = 1 kPa; (b) $s_{u0,d}$ = 5 kPa (seabed shear strength, $s_{u0,b}$ = 10 kPa)

**Table 4. 1.** Parameters used in numerical modelling for base case analysis and parametric study

| Parameters | Base case | Parametric study |
|---|---|---|
| Pipe diameter, $D$ (mm) | 290 | 290 |
| Pipe length, $L$ (mm) | 10 | 10 |
| Normalized depth of embedment, $\hat{w}$ | 3 | 3 |
| Normalized gap between pipe and seabed, $\hat{g}$ | 0.5 to 3.0 | 0.5 to 3.0 |
| Debris undrained shear strength prior to any softening, $s_{u0,d}$ (kPa) | 5 | 1, 3, 5 |
| Seabed undrained shear strength prior to any softening, $s_{u0,b}$ (kPa) | 10 | 2, 6, 10 |
| Saturated unit weight of clay, $\gamma_{sat}$ (kN/m$^3$) | 15.81 | 15.81 |
| Rate of increase of $s_u$ per log cycle, $\mu$ | 0.1 | 0.1 |
| Reference shear strain rate, $\dot{\gamma}_{ref}$ (s$^{-1}$) | $3 \times 10^{-6}$ | $3 \times 10^{-6}$ |
| Clay sensitivity, $S_t$ | 3 | 3 |
| Accumulated absolute plastic shear strain for 95% strength degradation, $\xi_{95}$ | 10 | 10 |
| Velocity of debris, $v_0$ (m/s) | 2 | 2 |
| Unit weight of water, $\gamma_w$ (kN/m$^3$) | 9.81 | 9.81 |
| Dynamic viscosity of water, $\mu_w$ (kg/(m/s)) | 0.00089 | 0.00089 |

# Chapter 5

# Conclusions and Future Recommendations

## 5.1 Conclusions

Submarine landslides can pose a significant threat to pipelines and seafloor structures. Complex pipe–soil–water interaction takes place when a failed soil mass impacts a suspended pipeline. The present study investigates a number of factors that influence the quantification of the drag force on free-span pipelines. The modeling of debris flow impact involves a number of challenging issues, including the extremely large deformation, role of water entrapped in the channel (free water) that forms behind the pipe during flow of soft clay around the pipe, and pipe–soil–water interface. The conventional finite element (FE) method based on Lagrangian framework cannot model such large deformation. Therefore, in the present study, the Coupled Eulerian–Lagrangian approach available in Abaqus FE software and a Computational Fluid Dynamics (CFD) approach available in ANSYS CFX are used. The effects of water are modelled in both FE and CFD analyses. For the interfaces, instead of using smooth/rough and fully-bonded/unbonded conditions as typically used in FE analysis, the interface behaviour is modelled using a concept similar to finite thickness interface element. The present study also models the interface resistance properly considering the surrounding materials (clay or water) outside the pipe surface. In Chapter 3, a comparison of the performance of two software packages is performed without considering strain-rate and strain-softening effects on clay shear strength. It is shown that the CFD approach in ANSYS CFX is computationally efficient than the CEL approach in Abaqus. Therefore, for further investigations, ANSYS CFX is used in Chapter 4. The strain-softening and strain-rate effects on undrained shear strength of clay are considered. The effects of debris and seabed shear

strength and gap ratio on the drag force are investigated. The main findings of this study can be summarized as follows:

i) Both Abaqus CEL and ANSYS CFX can model large deformation and effects of free-water suction on the pipeline; however, ANSYS CFX is more computationally efficient.

ii) A significant large penetration distance is required to mobilize the maximum drag force on the pipeline.

iii) The maximum normalized drag force on a suspended pipeline is significantly influenced by the suction due to free-water-suction developed behind the pipe which depends on gap ratio and shear strength of seabed and debris.

iv) In the case of lower gap ratios ($\hat{g} \leq 2$), the penetration distance required for mobilization of maximum drag force on the pipeline is lower than that in case of higher gap ratios ($\hat{g} \geq 2$).

v) A small gap ($\hat{g} \leq 2$) prevents the flow of debris material through the space beneath the pipe. This results in lower suction in the free water and thereby a lower normalized drag force. However, a combination of weaker seabed and small gap can alter the scenario.

vi) A high gap ratio ($\hat{g} \geq 2$) facilitates the formation of a closed channel behind the pipe and allows the development of free water suction. This causes a higher value of the normalized drag force.

## 5.2 Recommendations for future research

The phenomenon of pipe–soil–water interaction during the submarine landslide impact on suspended pipelines has been successfully simulated in the present study. However, this study has some limitations, which could be addressed in future studies.

- The numerical analyses presented in this study is only for a single burial depth (equal to three times of pipe diameter). Further investigation is required to check the effect of burial depth on the drag force.
- An improved modelling technique is needed to model the debris–seabed and debris–water interface. The reduction of shear strength of material near the debris–seabed interface, potentially due to strain-softening or water entrainment, could be considered.
- The numerically simulated results can be compared with new or available physical test results.
- A design chart for estimating the maximum drag force on the pipe can be proposed after conducting a comprehensive parametric study for varying embedment, velocity of debris, shear strength of seabed and debris and gap ratios.

# References

American Lifelines Alliance. Guidelines for the design of buried steel pipe. Federal Emergency Management Agency, USA, 2001:75.

Arnold, K.E. 1967. Soil movements and their effects on pipelines in the Mississippi delta region, PhD Thesis, Tulane University of Louisiana, New Orleans, Louisiana, USA.

Audibert, J.M., and Nyman, K.J. 1977. Soil restraint against horizontal motion of pipes. Journal of the Geotechnical Engineering Division, **103**(10): 1119–1142.

Bea, R. G., and Aurora, R. 1982. Design of pipelines in mudslide areas. *In* Proceedings of the 14th Annual Offshore Technology Conference, Houston, TX, USA, pp. 401–414.

Bearman, P.W., and Zdravkovich, M.M. 1978. Flow around a circular cylinder near a plane boundary. Journal of Fluid Mechanics, **89**(1): 33–47.

Bondevik, S., Løvholt, F., Harbitz, C., Mangerud, J., Dawson, A. and Svendsen, J.I. 2005. The Storegga slide Tsunami—comparing field observations with numerical simulations, Marine and Petroleum Geology, **25:** 195–208.

Boukpeti, N., White, D., Randolph, M. and Low, H.E. 2009. Characterization of the solid-fluid transition of fine-grained sediments. *In* 28th International Conference on Ocean, Offshore and Arctic Engineering, Honolulu, Hawaii, USA, May 31–June 5, pp. 293–303.

Boukpeti, N., White, D., Randolph, M., and Low, H. 2012. Strength of fine-grained soils at the solid–fluid transition. Géotechnique, **62**(3): 213–226.

Boylan, N., C. Gaudin, D. J. White, M. F. Randolph, and J. A. Schneider. 2009. Geotechnical centrifuge modelling techniques for submarine slides. *In* proceedings of the 28th international conference on ocean, offshore and arctic engineering, Honolulu, US, **7**, pp. 65–72.

Brookes, G.F., and Whitmore, R.L. 1968. The static drag on bodies in Bingham plastics. Rheologica Acta, **7**(2): 188–193.

Chi, K. F. 2012. Glide block or out-runner block impact on suspended submarine pipeline. Master's Thesis, Memorial University of Newfoundland, Canada.

De Blasio, F.V., Elverhøi, A., Issler, D., Harbitz, C.B., Bryn, P. and Lien, R. 2005. On the dynamics of subaqueous clay rich gravity mass flows—the giant Storegga slide, Norway. Marine and Petroleum Geology, **22**(1–2): 179–186.

Demars, K.R., Nacci, V.A., and Wang, W.D. 1977. Pipeline failure: a need for improved analyses and site surveys. Offshore Technology Conference, Houston, Texas, USA, **28**: 76–83.

Demars, K. R. (1978). Design of marine pipelines for areas of unstable sediment. ASCE Transportation Engineering Journal **104**(1): 109–112.

Dey, R., Hawlader, B., Phillips, R. and Soga, K. 2016. Modeling of large-deformation behaviour of marine sensitive clays and its application to submarine slope stability analysis. Canadian Geotechnical Journal, **53**(7): 1138–1155.

Drago, M., Mattioli, M., Bruschi, R. and Vitali, L. 2015. Insights on the design of free-spanning pipelines. Philosophical Transactions of the Royal Society A, **373**(2033): 20140111.

Dutta, S., and Hawlader, B. 2018. Pipeline–soil–water interaction modelling for submarine landslide impact on suspended offshore pipelines. Géotechnique,1–43.

Dutta, S., Hawlader, B., and Phillips, R. 2015. Vertical penetration of offshore pipelines: a comparative study between finite element and finite volume methods, International Conference on Ocean, Offshore and Arctic Engineering, ASME, pp. 0–10.

Einav, I., and Randolph, M. F. 2005. Combining upper bound and strain path methods for evaluating penetration resistance. International Journal for Numerical Methods in Engineering, **63**(14): 1991–2016.

Fine, I.V., Rabinovich, A.B., Bornhold, B.D., Thomson, R.E. and Kulikov, E.A. 2005. The Grand Banks landslide-generated Tsunami of November 18, 1929: preliminary analysis and numerical modelling. Marine Geology, **215**(1–2): 45–57.

Georgiadis, M. 1991. Landslide drag forces on pipelines. Soils and Foundations, **31**(1): 156–161.

Geöktun, S. 1975. The drag and lift characteristics of a cylinder placed near a plane surface, PhD Thesis, Naval Postgraduate School, Monterey, California.

Gui, M. W., and Bolton, M. D. (1998). Geometry and scale effects in CPT and pile design. *In* proceedings of the 1st International Conference on Geotechnical Site Characterization, Atlanta, GA, USA, pp. 1063–1068.

Hadj-Hamou, T., and Kavazanjian, E., Jr. 1985. Seismic stability of gentle infinite slopes, Journal of Geotechnical Engineering, **111**(6): 681–697.

Jiang, L. and LeBlond, P.H. 1993. Numerical modelling of an underwater Bingham plastic mudslide and the waves which it Generates. Journal of Geophysical Research: Oceans, **98**(C6): 10303–10317.

Jostad, H. P. and Andresen, L. 2004. Modelling of shear band propagation in clays using interface elements with finite thickness. In proceeding of the 9th International Symposium on Numerical Models in Geomechanics, Ottawa, Canada, **9**: pp. 121–128.

Kvalstad, T., Nadim, F. & Arbitz, C. (2001). Deepwater geohazards: Geotechnical concerns and solutions. In proceedings of the Offshore Technology Conference, TX, USA.

Lei, C., Cheng, L. and Kavanagh, K. 1999. Re-examination of the effect of a plane boundary on force and vortex shedding of a circular cylinder. Journal of Wind Engineering and Industrial Aerodynamics, **80**(3): 263–286.

Martin, C.M., and White, D.J. 2012. Limit analysis of the undrained bearing capacity of offshore pipelines. Géotechnique, **62**(9): 847–863.

Masson, D.G., Harbitz, C.B., Wynn, R.B., Pedersen, G., and Løvholt, F. 2006. Submarine landslides: processes, triggers and hazard prediction. Philosophical Transactions of the Royal Society of London A: Mathematical, Physical and Engineering Sciences, **364**(1845): 2009–2039.

Mulder, T., and Alexander, J. 2001. The physical character of subaqueous sedimentary density flows and their deposits. Sedimentology, **48**(2): 269-299.

Oliveira, J.R., Almeida, M.S., Almeida, M.C., and Borges, R.G. 2009. Physical modeling of lateral clay–pipe interaction. Journal of Geotechnical and Geoenvironmental Engineering, **136**(7): 950–956.

Paulin, M.J., Phillips, R. and Boivin, R., 1995. Centrifuge modelling of lateral pipeline/soil interaction--Phase 2 (No. CONF-950695--). American Society of Mechanical Engineers, New York, NY (United States).

Paulin, M.J., Phillips, R. and Boivin, R. 1996. An Experimental Investigation into Lateral Pipeline/Soil Interaction, International Conference on Offshore Mechanics Arctic Engineering, ASME, New York, USA.

Paulin, M. J., Phillips, R., Clark, J. I., and Boivin, R. 1998. An experimental investigation into lateral pipeline/soil interaction–Phase II. *In* proceedings of the International Conference on Centrifuge, Tokyo, Japan, pp. 699–704.

Pazwash, H., and Robertson, J. M. 1975. Forces on Bodies in Bingham Fluids. Journal of Hydraulic Research, **13**(1): 35–55.

Phillips, R., Nobahar, A., and Zhou, J. 2004. Trench Effects on Soil/Pipe Interaction. *In* proceedings of the 2004 International Pipeline Conference, New York, USA, pp. 321–327.

Pei, Y., Y. B. He, H. Li, and B. Xiao. 2015. Discuss about relationship between high-density turbidity current and sandy debris flow. Geological Review **61** (6):1281–92. (in Chinese).

Piper, D.J. 1988. The 1929 Grand Banks earthquakes, slump, and turbidity current. Geological Society of America, Special Paper, **229**: 77–92.

Piper, D.J., Cochonat, P., and Morrison, M.L. 1999. The Sequence of events around the epicentre of the 1929 Grand Banks earthquake: initiation of debris flow and turbidity current inferred from Sidescan Sonar. Sedimentology, **46**(1): 79–97.

Randolph, M. F., and White, D. J. 2012. Interaction forces between pipelines and submarine slides—a geotechnical viewpoint. Ocean Engineering, **48**: 32–37.

Roshko, A., Steinolfson, A., and Chattoorgoon, V. 1975. Flow forces on a cylinder near a wall or near another cylinder. California Institute of Technology, Pasadena, USA.

Saha, D., Hawlader, B., Dutta, S., and Dhar, A. 2018. A comparison using two numerical approaches for modelling the impact of submarine landslides on suspended pipelines. *In* proceedings of GeoEdmonton, 2018, Edmonton, AB, Canada.

Sahdi, F., Gaudin, C., White, D.J., Boylan, N. and Randolph, M.F. 2014. Centrifuge modelling of active slide-pipeline loading in soft clay. Géotechnique, **64**(1): 16–27.

Slingsby, M.J. 2015. Dynamic interaction of subsea pipeline spans due to vortex-induced vibrations. Master's Thesis, Delft University of Technology, Delft, Netherlands.

Summers, P.B., and Nyman, D.J. 1985. An approximate procedure for assessing the effects of mudslides on offshore pipelines. Journal of Energy Resources Technology, **107**(4): 426–432.

Supachawarote, C., Randolph, M., and Gourvenec, S. 2004. Inclined pull-out capacity of suction caissons. *In* the proceedings of fourteenth International Offshore and Polar Engineering Conference, May 23–28, 2004, Toulon, France.

Swanson, R. C. and Jones, W. T. (1982). Mudslide effects on offshore pipelines. ASCE Transportation Engineering Journal, **108**(6): 585–600.

Wang, D., Bienen, B., Nazem, M., Tian, Y., Zheng, J., Pucker, T., and Randolph, M. F. 2015. Large deformation finite element analyses in geotechnical engineering, Computers and Geotechnics, **65**: 104–114.

Yang, B., Jeng, D.S., Gao, F.P., and Wu, Y.X. 2008. Forces acting on the seabed around a pipeline in unidirectional ocean currents. Open Civil Engineering Journal, **2**:148–155.

Yuan, F., Wang, L., Guo, Z., and Xie, Y., 2012. A refined analytical model for landslide or debris flow impact on pipelines–Part II: Embedded pipelines. Applied Ocean Research, **35**:105–114.

Zakeri, A., Høeg, K., and Nadim, F. 2008. Submarine debris flow impact on pipelines—part I: experimental investigation. Coastal Engineering, **55**(12): 1209–1218.

Zakeri, A., Høeg, K., and Nadim, F. 2009. Submarine debris flow impact on pipelines—Part II: numerical analysis. Coastal Engineering, **56**(1): 1–10.

Zakeri, A. 2009. Review of the state-of-the-art: drag forces on submarine pipelines and piles caused by landslide or debris flow impact, Journal of Offshore Mechanics and Arctic Engineering, ASCE, **131**(1).

Zakeri, A., Hawlader, B., and Chi, K. 2012. Drag forces caused by submarine glide block or out-runner block impact on suspended (free-span) pipelines. Ocean Engineering, **47**: 50–57.

Zakeri, A., and Hawlader, B. 2013. Drag forces caused by submarine glide block or out-runner block impact on suspended (free-span) pipelines—numerical analysis. Ocean Engineering, **67**: 89–99.

Zhang, L., Zhao, X., Yan, X., and Yang, X. 2016. A semi-analytical method of stress-strain analysis of buried steel pipelines under submarine landslides. Applied Ocean Research, **59**: 38–52.

Zhu, H., and Randolph, M. F. 2009. Large deformation finite-element analysis of submarine landslide interaction with embedded pipelines. International Journal of Geomechanics, **10**(4): 145–152.